Journal of Sound and Vibration 329 (2010) 585–606

Contents lists available at ScienceDirect

Journal of Sound and Vibration

journal homepage: www.elsevier.com/locate/jsvi

Analysis of milling dynamics for simultaneously engaged cutting teeth

Oleg A. Bobrenkov [a,*], Firas A. Khasawneh [b], Eric A. Butcher [a], Brian P. Mann [b]

[a] Department of Mechanical and Aerospace Engineering, New Mexico State University, Las Cruces, NM 88003, USA
[b] Department of Mechanical Engineering and Materials Science, Duke University, Durham, NC 27708, USA

ARTICLE INFO

Article history:
Received 15 December 2008
Received in revised form
22 September 2009
Accepted 23 September 2009
Handling Editor: M.P. Cartmell
Available online 25 October 2009

ABSTRACT

This paper investigates the stability of a milling process with simultaneously engaged teeth and contrasts it to prior work for a single tooth in the cut. The stability analyses are performed with the Chebyshev collocation method and the state-space TFEA technique. These analyses show that a substantially different stability behavior is observed. In addition, the stability lobes are shown to undergo rapid transitions for relatively small changes in the radial immersion ratio; these transitions are explained in terms of the specific cutting force profiles. The stable periodic motion of the tool was also investigated using a harmonic balance approach and a dynamic map created with the TFEA technique. The findings suggest that a large number of harmonics are required for the harmonic balance approach to obtain the correct solution.

1. Introduction

Predictive models have become an important part of modern cutting operations. The integration of these models into cutting processes is largely driven by the increased competition for shorter production times and accurately machined surfaces. Although increasing the material removal rate reduces the machining time, the associating relative vibrations between the tool and the workpiece can become unstable. These unstable vibrations are commonly called chatter [1,2] and they could damage the tool, the fixture and/or the machine spindle [3–6]. Optimizing the machining process for maximum productivity and chatter-free cutting has been made possible by research advancements in modeling, solving, and analyzing the stability of machining operations in the process parameter space.

The research on machine-tool chatter was started by Taylor more than 100 years ago [7]. The early work that followed led to the introduction of stability diagrams which chart the boundary between stable and unstable cuts as a function of the spindle speed and depth of cut [2,8,9]. Crossing a stability boundary into an unstable region causes the tool to chatter with certain chatter frequencies. These frequencies are usually characterized by frequency diagrams which illustrate the chatter frequencies at the loss of stability [10,11]. Chatter frequencies can also be verified experimentally through analyzing the measured chatter signals [12–14].

Chatter in cutting processes has been explained as a consequence of regenerative effects. These effects are commonly modeled through delay-differential equations (DDEs) which lead to an infinite dimensional state-space [10] and to mechanistic cutting coefficients that are usually estimated experimentally [15]. For a limited class of DDEs, e.g. continuous turning, closed-form expressions for the stability boundaries can be obtained [10]. However, recent techniques, such as

* Corresponding author. Tel.: +1 575 646 3501; fax: +1 575 646 6111.
E-mail address: chaalis@nmsu.edu (O.A. Bobrenkov).

0022-460X/$ - see front matter © 2009 Elsevier Ltd. All rights reserved.
doi:10.1016/j.jsv.2009.09.032

semi-discretization [16,17], Chebyshev-based methods [18–20], collocation methods [21], temporal finite element analysis (TFEA) [22–25], D-partition method [26], and certain frequency domain techniques [27,28] have emerged as numerical and semi-analytical tools to determine the stability of more general DDEs. Numerical simulation is also used to study machining stability [14,29–31]; however, semi-analytical predictions of stability can quickly and accurately give stability regions over the process parameter space of interest making them superior to tedious numerical simulations [32–35].

The complexity of the DDE increases considerably if it contains both discontinuities in time and periodic coefficients. Milling, for instance, is one of the most common metal removal processes that is commonly approximated as a periodic, piece-wise continuous system. Therefore, an approximation scheme is typically necessary to determine milling stability. Although TFEA [5,24,25,36–38] and Chebyshev-based methods [39,40] have been separately used to analyze the stability of various applications, they have never been directly compared.

Another major difference between this paper and previous works is that we investigate the stability of a milling process with simultaneously engaged teeth. Fig. 1 illustrates the contrast between this work and prior research. In this figure, θ^{enter} is the entry angle, θ^{exit} is the exit angle, and for an evenly spaced cutter the pitch angle, ψ_p, is the uniform angle between the teeth. The typical case studied in the literature is shown in Fig. 1a which corresponds to $\theta^{\text{exit}}-\theta^{\text{enter}}\leq\psi_p$. No more than one tooth is in the cut over any tooth passage period τ and free vibration can occur over some finite time in τ. However, this study investigates the two other cases that arise with a multiple-tooth cutter and different radial immersions. More specifically, case (b) occurs when $\theta^{\text{exit}}-\theta^{\text{enter}}>\psi_p$ and $\theta^{\text{exit}}-\theta^{\text{enter}}\neq r\psi_p$, where r is an integer. In this case, multiple teeth will be in the cut simultaneously at some point in the delay period τ. However, the times for tooth entry and exit do not coincide such that the number of engaged teeth either increases or decreases by one. Case (c), on the other hand, corresponds to $\theta^{\text{exit}}-\theta^{\text{enter}}=r\psi_p$ and the number of the engaged teeth remains constant over τ since one tooth enters the cut at the same instant another exits. For example, this case arises for a 4-tooth cutter at full radial immersion or with a 3-tooth cutter at 75 percent radial immersion. For cases (b) and (c) no free vibration occurs over any portion of τ.

While many works have investigated case (a) and the geometry of multiple teeth has been discussed previously in [3,4], the stability features of cases (b) and (c) for *multiple engaged teeth*, especially as a function of radial immersion level, have not received much attention and are being analyzed for the first time here. However, it is common in industry to cut with many teeth at the same time—as in cases (b) and (c). This is especially the case when performing finishing cuts on hard materials, such as titanium. In addition, since multiple cutting teeth and low radial immersions are common in finish cuts, dimensional precision is exceptionally important for cases (b) and (c). However, a parameter selection scheme based entirely on stability considerations alone can still result in inaccurately machined surfaces. This is due to the influence of the process parameters on the amplitude and phase of the tool oscillations [24]. Therefore, studying the periodic motion of the tool during stable cutting can provide invaluable information when producing precision components.

Recent studies have shown that a new bifurcation phenomena can occur in highly intermittent cutting. Besides Neimark–Sacker or secondary Hopf bifurcations, period-doubling bifurcations have been analytically predicted in

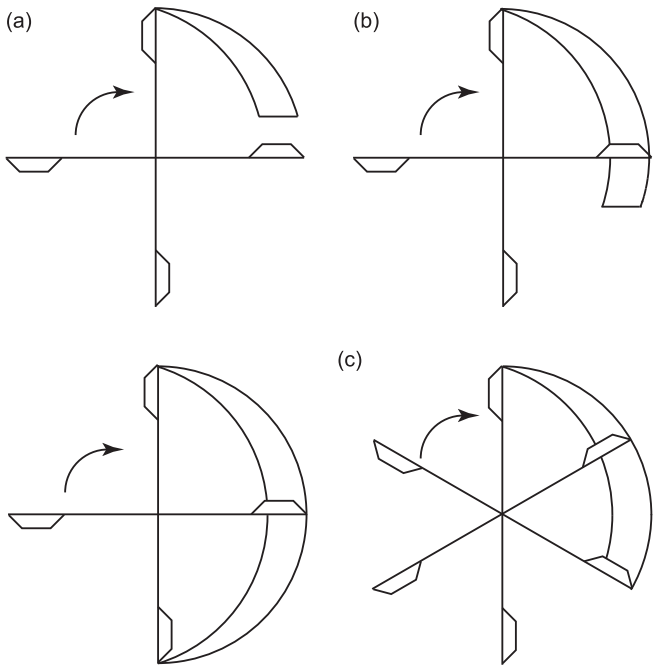

Fig. 1. The different cases to account for a multi-tooth cutter. In case (a), $\theta^{\text{exit}}-\theta^{\text{enter}}$ is less than the pitch angle; hence, only one tooth is in the cut at any time. On the other hand, in cases (b) and (c), $\theta^{\text{exit}}-\theta^{\text{enter}}$ is larger than the pitch angle; hence, multiple teeth will be cutting simultaneously.

Refs. [31,33,41–43] and confirmed experimentally in Refs. [11,25,36,44,45]. However, these previous works on milling bifurcations only investigated the case when a single tooth is engaged in cutting; a specific outcome from these works was that they found period-doubling at low radial immersions.

In this paper, we study the stability of a milling process with simultaneously engaged teeth by extending the Chebyshev collocation and the state-space TFEA techniques. The results of both techniques are validated through a series of overlaid stability diagrams which constitute the first direct comparison between these methods.

This work also shows substantially different stability behavior in comparison to prior results for a single tooth in the cut. More specifically, we observe the following new stability features: (1) a complete understanding of the manner in which an increased number of simultaneously engaged cutting teeth leads to disappearance of the period-doubling lobes and a qualitative similarity between the stability charts of multiple engaged teeth and those of the turning process. (Note that this is not shown in earlier studies where a simplified constant cutting force during tooth engagement [46,47] or constant-coefficient DDEs resulting from averaging of the periodic coefficients [32,35,48,49] are employed.), (2) a complete understanding of the effect of multiple engaged teeth on the shifting and reshaping of the entire instability lobes, and thus not only for the well-known shifts of their tips where they intersect the spindle speed axis by a factor of the number of cutting teeth, and (3) a contraction of the range of immersion levels for down-milling for which stability is maximized. This is shown through a series of stability diagrams for a down-milling process with different radial immersions and an increasing number of engaged teeth. The specific cutting force profiles, which give an indication of the changes in the cutting forces over one tooth passage period, are used to help explain this unusual stability behavior. The tool chatter frequency diagrams are also obtained to give the full stability picture.

The identification of rapid transitions in the stability lobes with relatively small changes in the radial immersion ratio is another difference between this work and prior results. This transition in the stability lobes is shown for a range of radial immersions and different multi-tooth cutters. An explanation for these transitions is presented using the average specific cutting force. The stable periodic motion of the tool is then studied using two different techniques: (1) a harmonic balance approach that approximates the cutting forces with a Fourier series, and (2) the TFEA approach through finding the fixed points of the dynamic map. The time series and the phase space results of both approaches are then compared and conclusions are drawn.

2. Milling model for multiple engaged teeth

This section examines a single degree-of-freedom milling model with a linear-regenerative cutting force. We consider the simultaneous engagement of multiple cutting teeth for up- and down-milling. This model has also been analyzed in [36,44,50,51] while higher degree-of-freedom versions were considered in [5,24,37], for example. The tool is assumed to be flexible in the x-direction only. A summation of cutting forces acting on the tool produces the equation of motion

$$\ddot{x}(t) + 2\zeta\omega_n\dot{x}(t) + \omega_n^2 x(t) = \frac{1}{m}\sum_{i=1}^{z} F_p(t), \tag{1}$$

where m is the mass, ζ is the damping ratio, ω_n is the natural frequency, and z is the number of teeth. According to Fig. 2a, the cutting force caused by the p th tooth $F_p(t)$ in the x-direction is given by

$$F_p(t) = g_p(t)(-F_{tp}(t)\cos\theta_p(t) - F_{np}(t)\sin\theta_p(t)), \tag{2}$$

where $\theta_p(t)$ is the angle of the p th cutting tooth, and $g_p(t)$ acts as a switching function. It is equal to one if the p th tooth is actively cutting and zero if it is not cutting; these time intervals are defined by the entry and exit angles which are specific to the cases of up- and down-milling (to be discussed). The tangential and normal force components are the products of the tangential and normal linearized cutting coefficients K_t and K_n, respectively, the nominal depth of cut b, and the

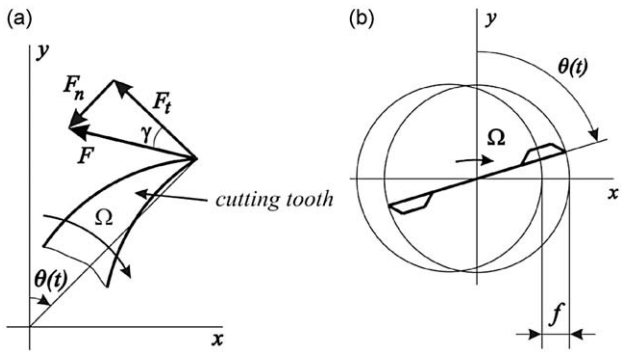

Fig. 2. Geometry of (a) cutting forces and (b) feed per tooth.

instantaneous chip width $w_p(t)$ as

$$F_{tp}(t) = K_t b w_p(t), \quad F_{np}(t) = K_n b w_p(t), \tag{3}$$

where

$$w_p(t) = f\sin\theta_p(t) + [x(t) - x(t-\tau)]\sin\theta_p(t) \tag{4}$$

depends on the feed per tooth f, the cutter angle $\theta_p(t)$, and the current and delayed tool position, see Fig. 2b. The tooth pass period in seconds is $\tau = 60/(z\Omega)$ [s] where Ω is the spindle speed given in rpm.

The substitution of Eqs. (3) and (4) into Eq. (2) yields

$$F_p(t) = -bK_t g_p(t)(\cos\theta_p(t) + \tan\gamma\sin\theta_p(t))\sin\theta_p(t)(f + x(t) - x(t-\tau)), \tag{5}$$

where $\tan\gamma = K_n/K_t$ (see Fig. 2a), and the angular position of the p th tooth is $\theta_p(t) = (2\pi\Omega/60)t + 2\pi(p-1)/z$.

Substituting (5) into (1) and summing over z teeth yields

$$\ddot{x}(t) + 2\zeta\omega_n\dot{x}(t) + \omega_n^2 x(t) = -\frac{bh(t)}{m}[x(t) - x(t-\tau)] - \frac{bf_0(t)}{m}, \tag{6}$$

where

$$h(t) = \sum_{p=1}^{z} K_t g_p(t)[\cos\theta_p(t) + \tan\gamma\sin\theta_p(t)]\sin\theta_p(t) \tag{7}$$

is the τ- periodic specific cutting force variation. Moreover, the expression for $f_0(t)$ is

$$f_0(t) = \sum_{p=1}^{z} K_t g_p(t)[\cos\theta_p(t) + \tan\gamma\sin\theta_p(t)]f\sin\theta_p(t). \tag{8}$$

The solution to Eq. (6) is assumed of the form

$$x(t) = \bar{x}(t) + \xi(t), \tag{9}$$

where $\bar{x}(t) = \bar{x}(t+\tau)$ is a τ- periodic solution that solves Eq. (6) and represents the unperturbed, ideal tool motion when no self-excited vibrations arise, and $\xi(t)$ is the perturbation. Substitution of Eq. (9) into Eq. (6) and elimination of terms involving $\bar{x}(t)$ and $f_0(t)$ yields

$$\ddot{\xi}(t) + 2\zeta\omega_n\dot{\xi}(t) + \omega_n^2\xi(t) = -\frac{bh(t)}{m}[\xi(t) - \xi(t-\tau)], \tag{10}$$

or in state space form

$$\frac{\mathrm{d}}{\mathrm{d}t}\begin{bmatrix}\xi\\ \dot{\xi}\end{bmatrix} = \begin{bmatrix}0 & 1\\ -\omega_n^2 - \dfrac{bh(t)}{m} & -2\zeta\omega_n\end{bmatrix}\begin{bmatrix}\xi\\ \dot{\xi}\end{bmatrix} + \begin{bmatrix}0 & 0\\ \dfrac{bh(t)}{m} & 0\end{bmatrix}\begin{bmatrix}\xi(t-\tau)\\ \dot{\xi}(t-\tau)\end{bmatrix}, \tag{11}$$

or

$$\dot{\boldsymbol{\xi}}(t) = \mathbf{R}(t)\boldsymbol{\xi}(t) + \mathbf{L}(t)\boldsymbol{\xi}(t-\tau), \tag{12}$$

where $\boldsymbol{\xi}(t)$ is a 2×1 state vector, $\mathbf{R}(t+\tau) = \mathbf{R}(t)$, and $\mathbf{L}(t+\tau) = \mathbf{L}(t)$. Eq. (12) is the linear variational DDE model of the milling process. Stability of the $\boldsymbol{\xi}(t) = \mathbf{0}$ solution in Eq. (12) implies the stability of the ideal (chatter-free) periodic motion $\bar{x}(t)$.

Two types of partial immersion processes are considered in this paper: up-milling and down-milling, see Fig. 3. In this figure, a is the radial depth of cut, D is the diameter of the tool while θ^{enter} and θ^{exit} are the entry and exit angles, respectively. These two angles can be characterized using the radial immersion a/D and they take different values for up-milling and down-milling processes. The dependence of the specific cutting force variation $h(t)$ on the entry and exit angles is attributed to the effect of the screen function $g_p(t)$ in Eq. (7). More specifically, for the pth tooth $g_p = 1$ if

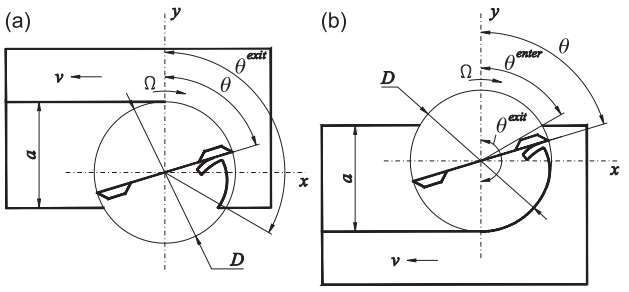

Fig. 3. Illustrations of (a) up-milling and (b) down-milling.

$\theta^{\text{enter}} < \theta_p < \theta^{\text{exit}}$ while $g_p = 0$ otherwise. The entry and exit angles can be found from Fig. 3 as $\theta^{\text{enter}} = 0$ and $\theta^{\text{exit}} = \cos^{-1}(1 - 2a/D)$ for up-milling, while for down-milling the angles are $\theta^{\text{enter}} = \cos^{-1}(2a/D - 1)$ and $\theta_p^{\text{exit}} = \pi$. These differences in the entry and exit angles in up-milling and down-milling lead to a different specific cutting force profile for the two processes which further separates the two with different dynamic behavior and stability properties.

The difference between the exit and entry angles gives the contact angle $\theta^{\text{contact}} = \cos^{-1}(1 - 2a/D)$. This angle describes the angular distance over which the tool is in contact with the workpiece in one spindle revolution. The percent time of the revolution that a single tooth is cutting is hence given by $\rho = \cos^{-1}(1 - 2a/D)/(2\pi)$. For a cutter with z teeth, this value is modified to $z\rho$ where—as long as $z\rho \le 1$—it now represents the percent of the revolution that all teeth are cutting. Otherwise, the case $z\rho > 1$ indicates simultaneously engaged teeth. This can also be extrapolated such that the condition for z_e simultaneously engaged teeth becomes $z\rho > z_e - 1$; or in terms of the radial immersion,

$$\frac{a}{D} > \sin^2 \frac{(z_e - 1)\pi}{z}. \tag{13}$$

For a z-tooth cutter, the maximum number of engaged teeth at full radial immersion is $z_e^{\max} = \lceil z\rho \rceil$, where $\lceil \cdot \rceil$ is the ceiling function (a function returning the smallest integer that is greater than or equal to its argument). However, since the maximum value of ρ for the full immersion case is 50 percent (see the case $z = 1$ in Fig. 4), the expression for the maximum number of engaged teeth becomes

$$z_e^{\max} = \lceil z\rho \rceil = \begin{cases} \dfrac{z}{2}, & z \text{ even}, \\ \dfrac{z+1}{2}, & z \text{ odd}. \end{cases} \tag{14}$$

Thus, multiple teeth can simultaneously engage in the cut only for $z > 2$. Specifically, for z = 3 or 4 there can be z_e = 1 or 2 engaged teeth, and $a/D = 75$ percent (for $z = 3$) and 50 percent (for $z = 4$) are the boundary cases. For $z = 6$, however, there can be $z_e = 1$, 2, or 3 engaged teeth, and the boundaries between these cases are at $a/D = 25$ and 75 percent. Fig. 5 shows this relation for several values of z_e and z.

Regardless of the number of teeth engaged in the cut, the milling process with a cutter of equally spaced teeth has τ- periodic coefficients and is therefore a τ- periodic process. This periodicity is shown in Fig. 6 for 4- and 6-tooth cutters. In graph (a) for a 4-tooth cutter, the starting position is repeated when tooth 2 takes the angular position of the reference tooth 1 after τ seconds from the beginning of the cut. A similar observation can be seen in graph (b) for a 6-tooth cutter. In general, for a cutter with any number of equally spaced teeth, periodicity is realized once every tooth passage period. Therefore, one way to look at the process is by assuming the revolution starts with the maximum possible number of teeth

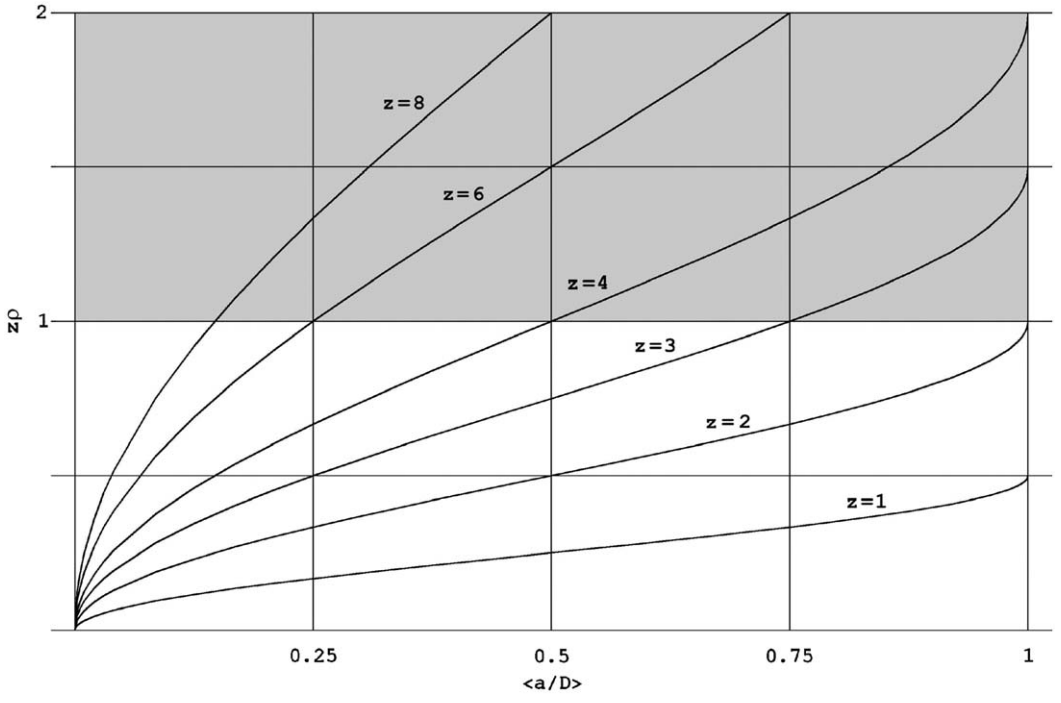

Fig. 4. Percent $z\rho$ of total time in the cut versus immersion ratio for various numbers of cutting teeth. The shaded portion corresponds to multiple engaged teeth.

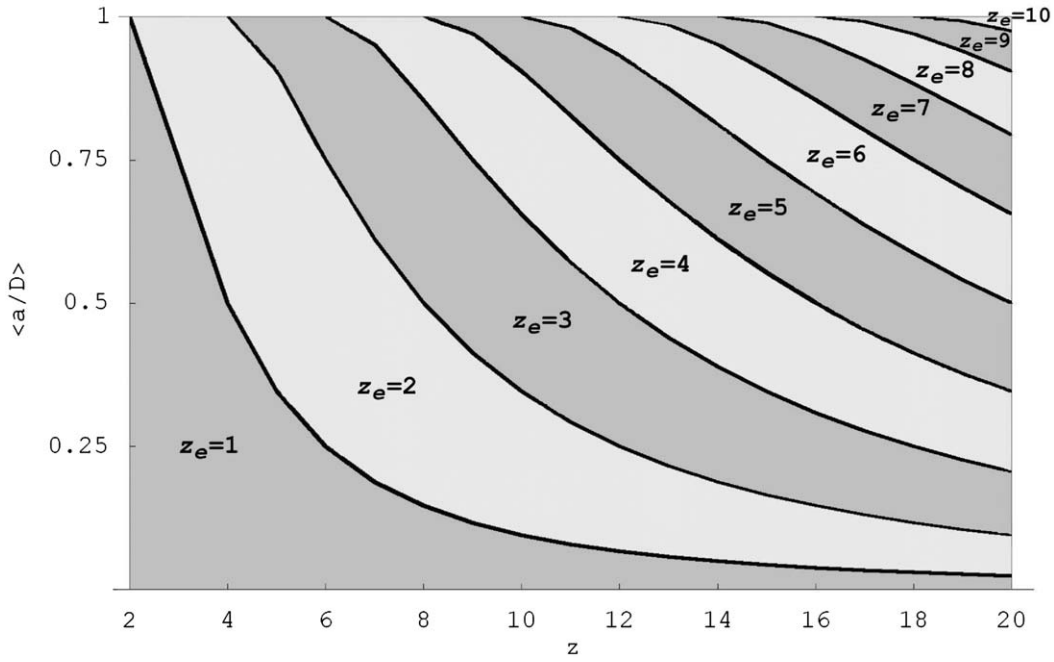

Fig. 5. Minimum radial immersion ratio for (bottom to top) $z_e = 1, 2, 3, 4, 5, 6, 7, 8, 9, 10$ multiple engaged cutting teeth versus total number of teeth z.

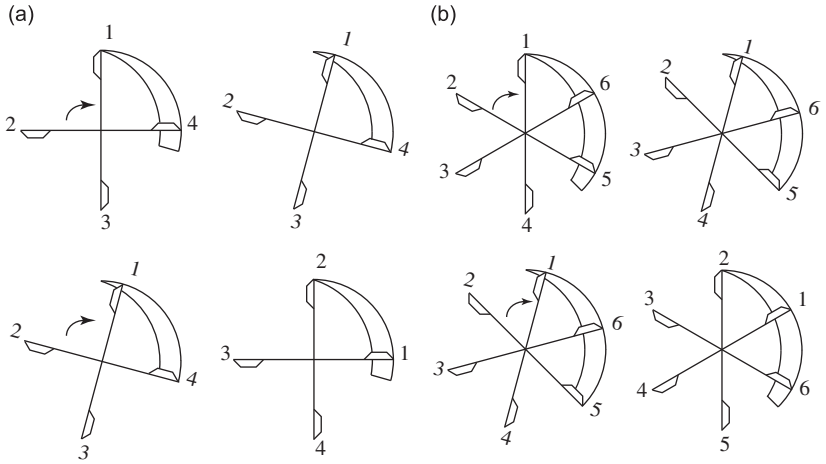

Fig. 6. The periodicity in a milling operation for (a) a 4-tooth cutter, and (b) a 6-tooth cutter.

engaged in the cut and then, depending on the radial immersion a/D and the number of teeth z, the leading tooth may exit the cut at some point during τ (see Fig. 6), before the same sequence repeats itself. Consequently, if a dynamic map is created for the state variable between two periods, Floquet theory can be used to determine stability. Two techniques to determine the stability of the linear periodic DDE in Eq. (12) are temporal finite element analysis (TFEA) [52] and Chebyshev collocation [53], which are introduced in the next two sections.

In both approaches, Eq. (12) is expressed as a map of the state vector $\boldsymbol{\xi}(t)$ in some basis (either temporal finite elements or Chebyshev collocation points) as $\mathbf{m}_{\xi}(i+1) = \mathbf{U}\mathbf{m}_{\xi}(i)$ or

$$\mathbf{m}_{i+1} = \mathbf{U}\mathbf{m}_i, \tag{15}$$

where $\mathbf{U}$ is a finite dimensional approximation of the infinite dimensional monodromy operator for time-periodic DDEs. Furthermore, the mapping equations will be obtained in the same form as (15) above. The dimensions of $\mathbf{m}_{\xi}$ and $\mathbf{U}$ are determined according to the desired level of accuracy, i.e. the number of finite elements or Chebyshev collocation points used. The eigenvalues of the monodromy operator $\mathbf{U}$ determine the system stability. In fact, the condition for asymptotic

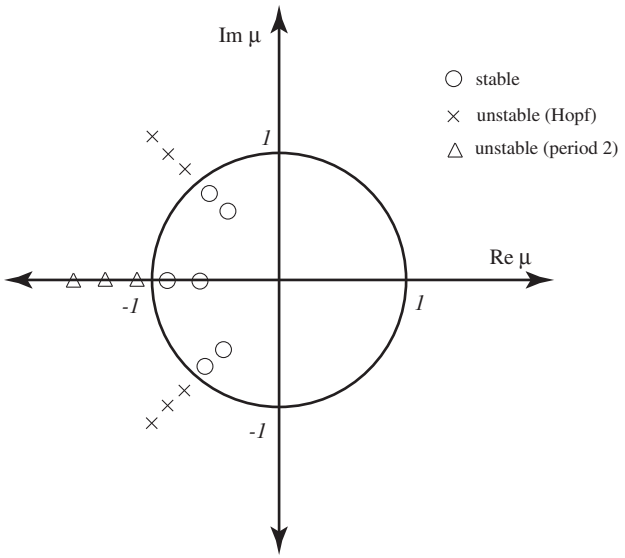

Fig. 7. The stability criteria dictates that all the eigenvalues, μ, of the monodromy operator **U**, should lie within the unit circle in the complex plane. Moreover, the manner in which the eigenvalues depart the unit circle produces different bifurcation behavior. For example, an eigenvalue leaving the unit circle through -1 results in a period-doubling bifurcation, whereas two complex conjugate eigenvalues departing the unit circle result in secondary Hopf bifurcation.

stability requires that all the characteristic multipliers, or eigenvalues of **U**, must lie within the unit circle of the complex plane, see Fig. 7.

3. Temporal finite element method

This section describes the stability analysis of Eq. (12) using temporal finite element analysis, or TFEA. The total time in the cut for one period is divided into temporal elements. Next, the expressions for the current state and the delayed state are approximated by a linear combination of trial functions $\phi(\sigma)$ during the j th element according to

$$\xi_j(t) = \sum_{i=1}^{3} \mathbf{a}_{ji}^{n} \phi_i(\sigma), \tag{16a}$$

$$\xi_j(t-\tau) = \sum_{i=1}^{3} \mathbf{a}_{ji}^{n-1} \phi_i(\sigma), \tag{16b}$$

where $\sigma \in [0, t_j]$ is the element local time and t_j is the length of the j th element. For example, if the total number of elements is E, then $t_j = \tau/E$ for elements of a uniform time. The chosen trial functions are obtained through interpolation and they are orthogonal on the interval $0 \le \sigma \le t_j$ [52]. Hence, the use of the local time notation ensures that they remain orthogonal for every temporal element. The set of trial functions used for this analysis is

$$\phi_1(\sigma) = 1 - 23\left(\frac{\sigma}{t_j}\right)^2 + 66\left(\frac{\sigma}{t_j}\right)^3 - 68\left(\frac{\sigma}{t_j}\right)^4 + 24\left(\frac{\sigma}{t_j}\right)^5, \tag{17a}$$

$$\phi_2(\sigma) = 16\left(\frac{\sigma}{t_j}\right)^2 - 32\left(\frac{\sigma}{t_j}\right)^3 + 16\left(\frac{\sigma}{t_j}\right)^4, \tag{17b}$$

$$\phi_3(\sigma) = 7\left(\frac{\sigma}{t_j}\right)^2 - 34\left(\frac{\sigma}{t_j}\right)^3 + 52\left(\frac{\sigma}{t_j}\right)^4 - 24\left(\frac{\sigma}{t_j}\right)^5. \tag{17c}$$

These functions are constructed such that the coefficients of the assumed solution directly represent the state variable at the beginning, middle and end of each temporal element, i.e. at $\sigma = 0$, $t_j/2$ and t_j, respectively. This is illustrated in the time line of Fig. 8 where the time in the current period n and the previous period $n-1$ is discretized into two elements for demonstration. Further, the dark dots represent the coefficients of the assumed solution which coincide with the actual solution $x(t)$ at discrete points in time.

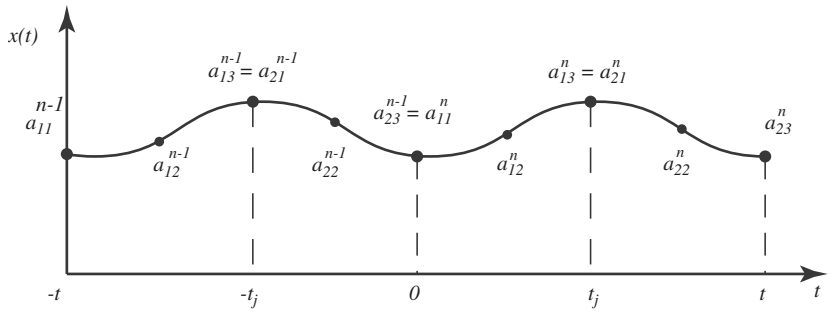

Fig. 8. Time line for the state variable $x(t)$ over a time interval of 2τ. The dark dots represent the points where the coefficients of the assumed solution coincide with the state variable. Moreover, the dashed lines mark the beginning and the end of each time element.

Consistent with Fig. 8, the following TFEA is presented using two elements. The corresponding form of the assumed solution is substituted into Eq. (12) which gives

$$\sum_{i=1}^{3}(\dot{\phi}_i(\sigma)\mathbf{a}_{ji}^{n} - \mathbf{R}(\sigma+(j-1)t_j)\phi_i(\sigma)\mathbf{a}_{ji}^{n} - \mathbf{L}(\sigma+(j-1)t_j)\phi_i(\sigma)\mathbf{a}_{ji}^{n-1}) = \text{error}, \tag{18}$$

where the error incurred in Eq. (18) is due to the approximation procedure. This error is minimized using the method of weighted residuals. Thus, Eq. (18) is multiplied by linearly independent weighting functions and the integral of the weighted error is set to zero. In this analysis, shifted Legendre polynomials are used since they satisfy the linear independence condition. More specifically, only the first two shifted Legendre polynomials $\psi_1(\sigma)=1$ and $\psi_2(\sigma)=2(\sigma/t_j)-1$ are used to keep the matrices square. Therefore, the weighted residual expression becomes

$$\sum_{i=1}^{3}\int_0^{t_j}(\dot{\phi}_i(\sigma)\mathbf{a}_{ji}^{n} - \mathbf{R}(\sigma+(j-1)t_j)\phi_i(\sigma)\mathbf{a}_{ji}^{n} - \mathbf{L}(\sigma+(j-1)t_j)\phi_i(\sigma)\mathbf{a}_{ji}^{n-1})\psi_p(\sigma)\,\mathrm{d}\sigma = 0. \tag{19}$$

Eq. (19) can be rearranged by collecting the terms that are multiplied by $\mathbf{a}_{ji}^{n}$ and the terms that are multiplied by $\mathbf{a}_{ji}^{n-1}$ in two different matrices:

$$\mathbf{N}_{pi}^{j} = \int_0^{t_j}(\mathbf{I}\phi_i(\sigma) - \mathbf{R}(\sigma+(j-1)tj)\phi_i(\sigma))\psi_p(\sigma)\,\mathrm{d}\sigma, \tag{20a}$$

$$\mathbf{P}_{pi}^{j} = \int_0^{t_j}\mathbf{L}(\sigma+(j-1)tj)\phi_i(\sigma)\psi_p\,\mathrm{d}\sigma, \tag{20b}$$

where $\mathbf{I}$ is an identity matrix, $\mathbf{N}_{pi}^{j}$ is the matrix containing the terms that are multiplied by $\mathbf{a}_{ji}^{n}$, while $\mathbf{P}_{pi}^{j}$ is the matrix containing the terms that are multiplied by $\mathbf{a}_{ji}^{n-1}$. These two terms are then used to populate two matrices on the opposite sides of Eq. (19) according to

$$\begin{bmatrix} \mathbf{I} & 0 & 0 & 0 & 0 \\ \mathbf{N}_{11}^{1} & \mathbf{N}_{12}^{1} & \mathbf{N}_{13}^{1} & 0 & 0 \\ \mathbf{N}_{21}^{1} & \mathbf{N}_{22}^{1} & \mathbf{N}_{23}^{1} & 0 & 0 \\ 0 & 0 & \mathbf{N}_{11}^{2} & \mathbf{N}_{12}^{2} & \mathbf{N}_{13}^{2} \\ 0 & 0 & \mathbf{N}_{21}^{2} & \mathbf{N}_{22}^{2} & \mathbf{N}_{23}^{2} \end{bmatrix} \begin{bmatrix} a_{11} \\ a_{12} \\ a_{21} \\ a_{22} \\ a_{23} \end{bmatrix}^{n} = \begin{bmatrix} 0 & 0 & 0 & 0 & \mathbf{\Phi} \\ \mathbf{P}_{11}^{1} & \mathbf{P}_{12}^{1} & \mathbf{P}_{13}^{1} & 0 & 0 \\ \mathbf{P}_{21}^{1} & \mathbf{P}_{22}^{1} & \mathbf{P}_{23}^{1} & 0 & 0 \\ 0 & 0 & \mathbf{P}_{11}^{2} & \mathbf{P}_{12}^{2} & \mathbf{P}_{13}^{2} \\ 0 & 0 & \mathbf{P}_{21}^{2} & \mathbf{P}_{22}^{2} & \mathbf{P}_{23}^{2} \end{bmatrix} \begin{bmatrix} a_{11} \\ a_{12} \\ a_{21} \\ a_{22} \\ a_{23} \end{bmatrix}^{n-1}, \tag{21}$$

which can be written in a more compact form as

$$\mathbf{H}\mathbf{a}_n = \mathbf{G}\mathbf{a}_{n-1}, \tag{22}$$

where $\mathbf{I}$ is an identity matrix and $\mathbf{\Phi}$ is the state transition matrix

$$\mathbf{\Phi} = \frac{1}{\lambda_1-\lambda_2}\begin{bmatrix} \lambda_1 e^{\lambda_2 t_f} - \lambda_2 e^{\lambda_1 t_f} & e^{\lambda_1 t_f} - e^{\lambda_2 t_f} \\ \lambda_1\lambda_2 e^{\lambda_2 t_f} - \lambda_1\lambda_2 e^{\lambda_1 t_f} & \lambda_1 e^{\lambda_1 t_f} - \lambda_2 e^{\lambda_2 t_f} \end{bmatrix}, \tag{23}$$

where $\lambda_{1,2} = -\zeta\omega_n \pm \omega_n\sqrt{\zeta^2-1}$, and t_f is the duration of free vibration. This state transition matrix relates the state of the tool as it exits the cut to its state as it re-enters the cut [54].

Recalling that the coefficients of the assumed solution directly represent the state variable at the beginning, middle, and end of each element, the coefficients vectors can be replaced with the actual state variable vectors and a dynamic map can be written as

$$\mathbf{H}\mathbf{m}_n = \mathbf{G}\mathbf{m}_{n-1}. \tag{24}$$

Therefore, in accordance with (15), the monodromy operator **U** is defined for TFEA as follows:

$$\mathbf{U} = \mathbf{H}^{-1}\mathbf{G}. \tag{25}$$

For more details about this technique and for convergence properties the reader is referred to Ref. [52].

4. Chebyshev collocation method

The Chebyshev collocation method is based on the properties of the Chebyshev polynomials of the first kind [55]. The Chebyshev collocation points are unevenly spaced points in the domain $[-1, 1]$ corresponding to the extremum points of the Chebyshev polynomial of degree N. As seen in Fig. 9a, we can also define these points as the projections of equispaced points on the upper half of the unit circle as $t_j = \cos(j\pi/N)$, $j = 0, 1, \ldots, N$ where the number of collocation points used is $m = N + 1$. A spectral differentiation matrix for the Chebyshev collocation points is obtained by interpolating a polynomial through the collocation points, differentiating that polynomial, and then evaluating the resulting polynomial at the collocation points [56]. We can find the differentiation matrix **D** for any order m as follows: let the rows and columns of the $m \times m$ Chebyshev spectral differentiation matrix **D** be indexed from 0 to N. The entries of this matrix are

$$D_{00} = \frac{2N^2+1}{6}, \quad D_{NN} = -\frac{2N^2+1}{6}, \quad D_{jj} = \frac{-t_j}{2(1-t_j^2)}, \ j = 1, \ldots, N-1,$$

$$D_{ij} = \frac{c_i(-1)^{i+j}}{c_i(t_i - t_j)}, \quad i \neq j, \ i,j = 0, \ldots, N, \ c_i = \begin{cases} 2, & i = 0, N, \\ 1 & \text{otherwise.} \end{cases} \tag{26}$$

The dimension of **D** is $m \times m$. Also let the $mq \times mq$ differential operator $\mathbb{D}$ (corresponding to q first-order DDEs) be defined as $\mathbb{D} = \mathbf{D} \otimes I_q$. Now let us approximate Eq. (12) using the Chebyshev collocation method, in which the approximate solution is defined by the function values at the collocation points in any given interval. (Note that for a collocation expansion on an interval of length $T = \tau$, the standard interval $[-1, 1]$ for the Chebyshev polynomials is easily rescaled.)

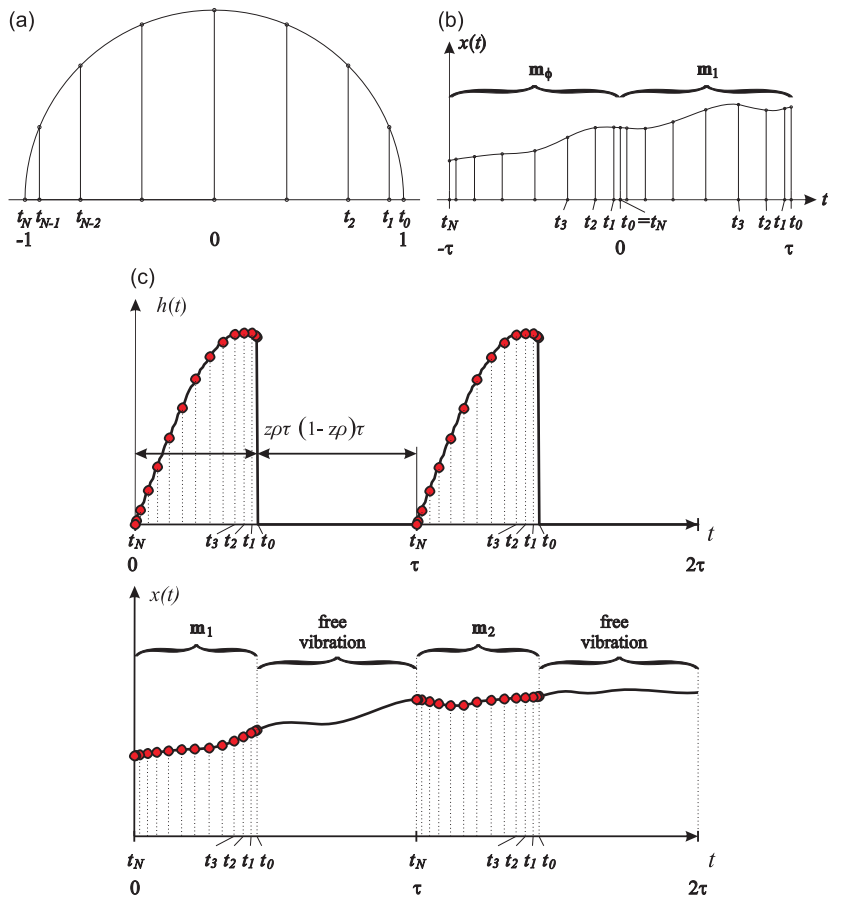

Fig. 9. Diagrams of (a) Chebyshev collocation points as defined by projections from the unit circle, (b) collocation vectors on successive intervals, and (c) collocation vectors for the case of a period of free vibration.

As shown in Fig. 9b, let $\mathbf{m}_1$ be the set of m values of $\xi(t)$ in the interval $t \in [0,T]$ and $\mathbf{m}_\phi$ be the set of m values of the initial function $\phi(t)$ in $t \in [-T,0]$. Recalling that the points are numbered from right to left by convention, the matching condition in Fig. 9b is seen to be that $\mathbf{m}_{1N} = \mathbf{m}_{\phi 0}$. Writing Eq. (12) in the algebraic form representing the Chebyshev collocation expansion vectors $\mathbf{m}_\phi$ and $\mathbf{m}_1$, we obtain

$$\hat{\mathbf{D}}\mathbf{m}_1 = \hat{\mathbf{M}}_R\mathbf{m}_1 + \hat{\mathbf{M}}_L\mathbf{m}_\phi. \tag{27}$$

In order to enforce the q matching conditions, the matrix $\hat{\mathbf{D}}$ is obtained from $\mathbb{D}$ by (1) scaling to account for the shift $[-1,1]\rightarrow[0,T]$ by multiplying the resulting matrix by $2/T$, and (2) modifying the last q rows as $[\mathbf{0}_q\ \mathbf{0}_q\ \ldots\ \mathbf{I}_q]$ where $\mathbf{0}_q$ and $\mathbf{I}_q$ are $q \times q$ null and identity matrices, respectively. The pattern of the product operational matrices is

$$\hat{\mathbf{M}}_R = \begin{bmatrix} \mathbf{R}(t_0) & & & & \\ & \mathbf{R}(t_1) & & & \\ & & \ddots & & \\ & & & \mathbf{R}(t_{N-1}) & \\ \mathbf{0}_q & \mathbf{0}_q & \cdots & \mathbf{0}_q & \mathbf{0}_q \end{bmatrix}, \tag{28}$$

where $\mathbf{R}(t_i)$ is calculated at the i th point on the interval of length τ. Similarly,

$$\hat{\mathbf{M}}_L = \begin{bmatrix} \mathbf{L}(t_0) & & & & \\ & \mathbf{L}(t_1) & & & \\ & & \ddots & & \\ & & & \mathbf{L}(t_{N-1}) & \\ \mathbf{I}_q & \mathbf{0}_q & \cdots & \mathbf{0}_q & \mathbf{0}_q \end{bmatrix}. \tag{29}$$

In Eq. (29), the hat ($\hat{}$) above the operator refers to the fact that the matrices are modified by altering the last q rows to account for the matching conditions.

In the case where only one tooth cuts at a time, there is in general some period between the cuts of free vibration corresponding to the system $\dot{\xi}(t) = \mathbf{R}_0\xi(t)$ where $\mathbf{R}_0 = \mathbf{R}(t)$ in Eqs. (11) and (12) when $h(t) = 0$. The state transition matrix $\mathbf{\Phi}(t)$ (see Eq. (23) in Section 3) that satisfies $\dot{\mathbf{\Phi}}(t) = \mathbf{R}_0\mathbf{\Phi}(t)$ can easily be found, from which the matching condition becomes $\mathbf{m}_{1N} = \mathbf{\Phi}((1-z\rho)\tau)\mathbf{m}_{\phi 0}$ (see Fig. 9c). Therefore, the last q rows of $\hat{\mathbf{M}}_L$ are changed to $[\mathbf{\Phi}((1-z\rho)\tau)\ \mathbf{0}_q\ \mathbf{0}_q\ \ldots]$.

In general, if inequality (13) is not satisfied with $z_e = 1$, then a portion of the delay period of length $z\rho\tau$ is approximated with Chebyshev collocation points (see the first diagram in the last row of Fig. 11), while the remainder of the period corresponds to free vibration. To account for the shift $[-1,1]\rightarrow[0,z\rho\tau]$, matrix $\hat{\mathbf{D}}$ in Eq. (27) is rescaled by multiplying $\mathbb{D}$ by $2/(z\rho\tau)$. If the immersion ratio is such that the inequality (13) becomes equality (which represents the borderline case between one and two engaged teeth), the length of the approximated portion becomes τ, as in the second diagram of the last row of Fig. 11 and the first diagram of the last row of Fig. 12. In this case the state transition matrix becomes identity, so the $\hat{\mathbf{M}}_L$ matrix becomes as in Eq. (29). Higher values of a/D such that inequality (13) is satisfied also result in the approximation of the entire delay period.

If the specific cutting force has a part of nonsmoothness on the interval of length τ, two separate expansions can be used for greater accuracy. This affects the structure of spectral differentiation and product operational matrices, such as in Eq. (27). Rewriting the vectors $\mathbf{m}_1$ and $\mathbf{m}_\phi$ as

$$\mathbf{m}_1 = \begin{bmatrix} \xi(t_{10}) \\ \vdots \\ \xi(t_{1N}) = \xi(t_{20}) \\ \vdots \\ \xi(t_{2N}) \end{bmatrix}, \quad \mathbf{m}_\phi = \begin{bmatrix} \phi(t_{10}) \\ \vdots \\ \phi(t_{1N}) = \phi(t_{20}) \\ \vdots \\ \phi(t_{2N}) \end{bmatrix}, \tag{30}$$

where t_{1j} and t_{2j} are the collocation points in the two portions of the expanded interval, we have the $\hat{\mathbf{D}}$ matrix in Eq. (27) written as

$$\hat{\mathbf{D}} = \begin{bmatrix} \left[\frac{2}{h_1}\mathbb{D}^{(1,Nq)}\right] & & & & \\ & & & \left[\frac{2}{h_2}\mathbb{D}^{(1,Nq)}\right] & \\ \mathbf{0}_q & \mathbf{0}_q & \cdots & \mathbf{0}_q & \mathbf{I}_q \end{bmatrix}, \tag{31}$$

where h_1 and h_2 are the lengths of the expanded portions and the superscript $(1, Nq)$ on $\mathbb{D}$ refers to the fact that only rows of $\mathbb{D}$ between 1 and Nq are written into the corresponding block. The $\hat{\mathbf{M}}_R$ and $\hat{\mathbf{M}}_L$ matrices are now expressed as

$$\hat{\mathbf{M}}_R = \begin{bmatrix} \mathbf{R}(t_{10}) & & & & \\ & \ddots & & & \\ & & \mathbf{R}(t_{1N}) = \mathbf{R}(t_{20}) & & \\ & & & \ddots & \\ & & & & \mathbf{R}(t_{1N-1}) \\ \mathbf{0}_q & \mathbf{0}_q & \cdots & \mathbf{0}_q & \mathbf{0}_q \end{bmatrix},$$

$$\hat{\mathbf{M}}_L = \begin{bmatrix} \mathbf{L}(t_{10}) & & & & \\ & \ddots & & & \\ & & \mathbf{L}(t_{1N}) = \mathbf{L}(t_{20}) & & \\ & & & \ddots & \\ & & & & \mathbf{L}(t_{1N-1}) \\ \mathbf{I}_q & \mathbf{0}_q & \cdots & \mathbf{0}_q & \mathbf{0}_q \end{bmatrix}. \tag{32}$$

Use of multiple interval collocation expansion will be applied to two specific cases of multiple engaged teeth.

Therefore, rearranging Eq. (27) and letting $\mathbf{m}_1 = \mathbf{m}_{i+1}$ and $\mathbf{m}_\phi = \mathbf{m}_i$, the map in Eq. (15) is obtained where the approximation to the monodromy operator is

$$\mathbf{U} = [\hat{\mathbf{D}} - \hat{\mathbf{M}}_R]^{-1}\hat{\mathbf{M}}_L. \tag{33}$$

It is seen that if m is the number of collocation points in each interval and q is the size of the first-order DDE of Eq. (12), then the size of the $\mathbf{U}$ matrix (whose eigenvalues approximate the Floquet multipliers which are largest in absolute value) for one Chebyshev interval will be $mq \times mq$ and for two intervals is $(2m-1)q \times (2m-1)q$. We can achieve higher accuracy of the Floquet multipliers by increasing the value of m. A MATLAB suite of codes called DDEC which computes stability boundaries for linear periodic DDEs with multiple discrete delays has been written and is available for download [57]. Other than for linear stability analysis of periodic DDEs including the milling model [39,40], this collocation method has also been used for center manifold reduction of nonlinear periodic DDEs [58] and parameter identification of periodic nonlinear ODEs [59]. For more details on the Chebyshev collocation method and its convergence properties, see [56].

5. Discussion of stability results

The stability charts of Figs. 10–14 show the substantial stability changes that occur when multiple cutting teeth are engaged. In particular, the following important changes are observed: (1) a smooth disappearance of the period-doubling lobes as the number of simultaneously engaged cutting teeth is increased leading to a qualitative similarity between the stability charts of multiple engaged teeth and those of the turning process, (2) the well-known shifts of the tips of the unstable lobes where they intersect the spindle speed axis by a factor of the number of cutting teeth as well as a complete understanding of the shifting and reshaping of the entire instability lobes which do not conform to this rule, and (3) a contraction of the range of immersion levels for down-milling in the vicinity of the immersion level where the average cutting force for down-milling is zero for which stability is maximized. In addition, it will be seen in Fig. 5 that the specific cutting force for 100 percent immersion becomes constant only for an even number of teeth greater than or equal to 4.

The stability charts in Fig. 10 are obtained using TFEA and the Chebyshev collocation method for up-milling and down-milling processes with several immersion ratios and numbers of cutting teeth. The region above the stability boundaries indicates chatter, or unstable cutting, while the region below the boundaries represents stable, or chatter-free, cutting. The two techniques are shown to give practically identical results which validates the stability analysis. The system parameters used to construct these charts are shown in Table 1. Since 25 collocation points and 12 finite elements were used, the dimensions of the $\mathbf{U}$ matrix approximating the monodromy operator in Eq. (15) is 50×50 for Chebyshev collocation and 22×22 for TFEA. The eigenvalues of the monodromy operator determine the system stability when using either TFEA or collocation methods, see the stability criteria in Fig. 7. Moreover, the manner in which the eigenvalues depart the unit circle produces different bifurcation behavior. For example, an eigenvalue leaving the unit circle through -1 results in a period-doubling bifurcation, whereas two complex conjugate eigenvalues departing the unit circle results in secondary Hopf bifurcation. A cycle-fold bifurcation, which is associated with the case $\mu = 1$, cannot occur for an evenly spaced mill as was shown in Refs. [36,46,50]; however, cycle-fold bifurcations have been reported for variable pitch tools [60].

The type of bifurcation associated with unstable cutting is identified in Figs. 10–12; the regions of secondary Hopf bifurcation are indicated by an "H", while flip or period-doubling bifurcation is indicated by a "P". It can be seen that the stability charts obtained by TFEA and Chebyshev collocation are almost identical. It can be seen in Fig. 10 that the relative orientation of the Hopf and flip regions remains the same for all cases. However, the flip regions which are visible for the case of one tooth become smaller for 4, 6, and even smaller still for 10 teeth. In fact, this "disappearance" of flip regions is a typical characteristic in stability charts for mills with more simultaneously engaged cutting teeth. The reason can be

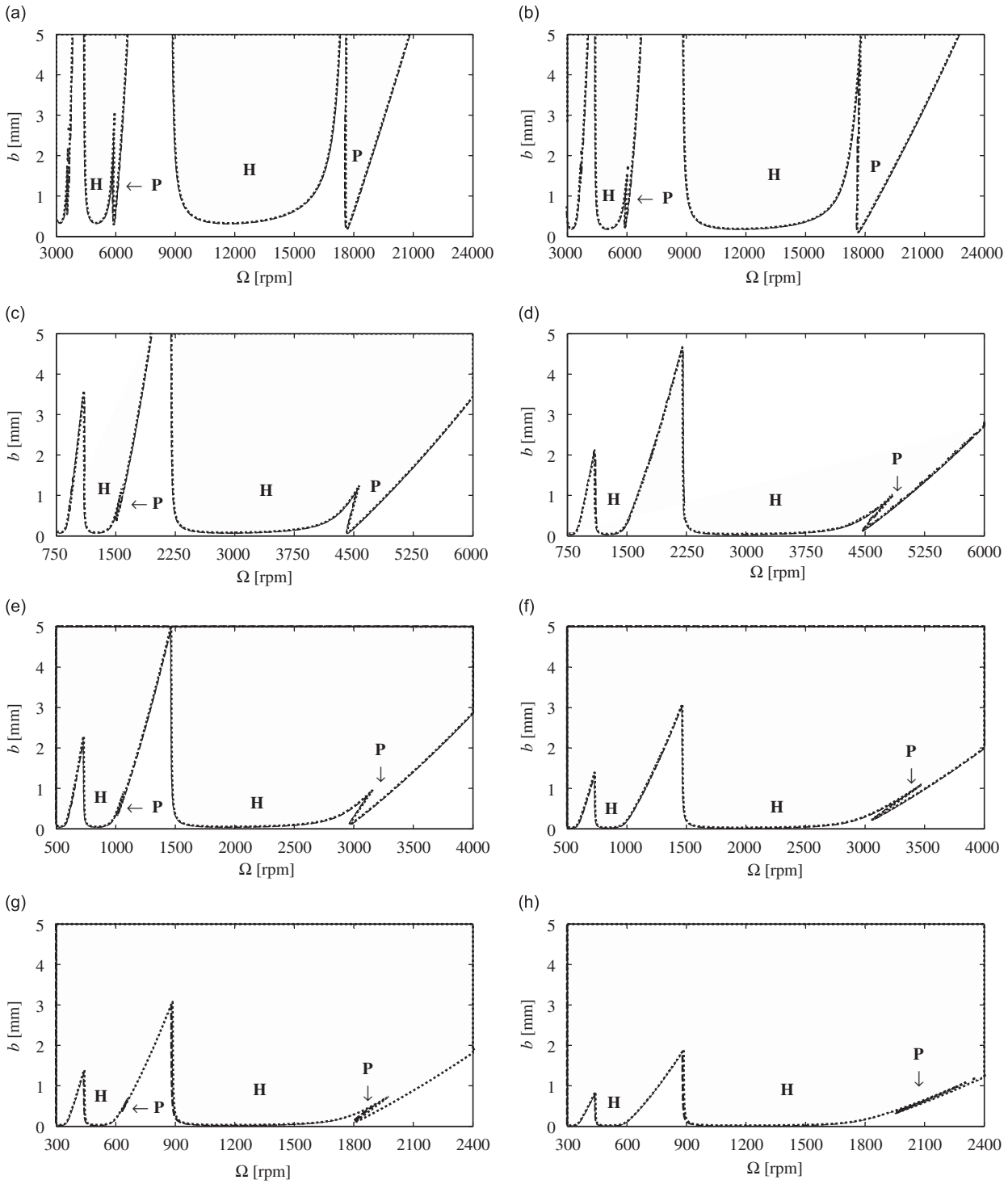

Fig. 10. Stability charts obtained with Chebyshev collocation method (dashed) and TFEA (dotted) for up-milling. The two columns were generated with the radial immersions 25 and 75 percent, respectively, and for cutters with: 1 tooth (row 1), 4 teeth (row 2), 6 teeth (row 3), and 10 teeth (row 4). The plane is discretized into a 300×300 grid for Chebyshev collocation method and a 600×600 grid for TFEA. Although the stability charts show similar qualitative features, note the shift in scales for the Ω- axis.

attributed to the fact that the flip regions are associated with discontinuities and higher harmonics in the specific cutting force profile, which vanish as the presence of a larger number of teeth begins to resemble the case of turning with a constant specific cutting force profile.

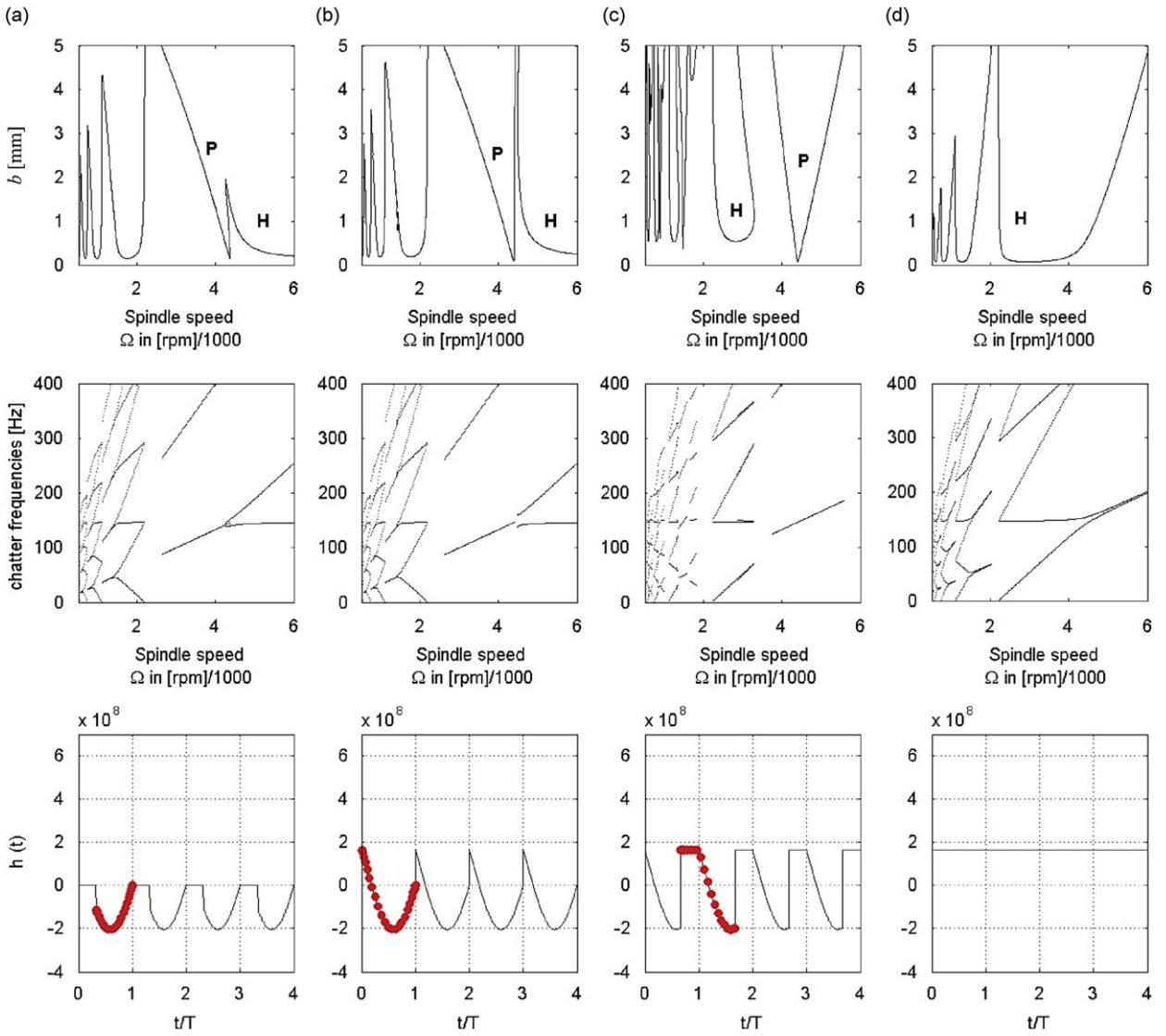

Fig. 11. Stability charts (first row), chatter frequencies (second row), and corresponding specific cutting force profiles (third row, where the thick line represents the segment that is approximated with Chebyshev collocation points) for 4 teeth, down-milling, and for $a/D = 0.25$ (column (a)), 0.50 (column (b)), 0.75 (column (c)), and 1 (column (d)).

The disappearance of the flip regions is also apparent in Figs. 11 and 12 for down-milling with 4 and 6 teeth, respectively. In these figures, a series of plots with increasing radial immersion shows prominent period-doubling lobes becoming smaller for 6 teeth compared to the case of 4 teeth over the whole partial radial immersion range. The stability charts for 4 teeth in Fig. 11 for 25, 50, 75, and 100 percent immersion ratios correspond to the cases (a), (c), (b), and (c), respectively, as shown in Fig. 1. Similarly, the results for the same immersion ratios in Fig. 12 correspond to the cases (c), (b), (c), and (c), respectively, in Fig. 1. Therefore, there are simultaneously engaged cutting teeth with the difference between the exit and entry angles being an integer multiple of the pitch angle in most cases. The case of full radial immersion, $a/D = 1$, results in a constant contact force due to the effect of superimposing the specific cutting forces of 4 and 6 teeth which are out of phase by $2\pi/z\Omega$. Therefore, only secondary Hopf instabilities are present in these cases as in the turning process. Note that for even higher numbers of cutting teeth, the specific cutting force approaches a constant value and the period-doubling lobes disappear for lower levels of radial immersion.

Some features similar to those in [40] can be observed for the down-milling cases in Figs. 11 and 12. In both figures, the specific cutting force (see the bottom rows) is always negative for low immersion ratios, and it begins to include some intervals of positive values at some value of immersion ratio below 50 percent for 4 teeth and below 75 percent for 6 teeth. In the down-milling stability charts (see the first rows of each figure), it can be observed that the mutual orientation of the secondary Hopf and period-doubling bifurcation stability lobes remains the same up to some value of the immersion ratio,

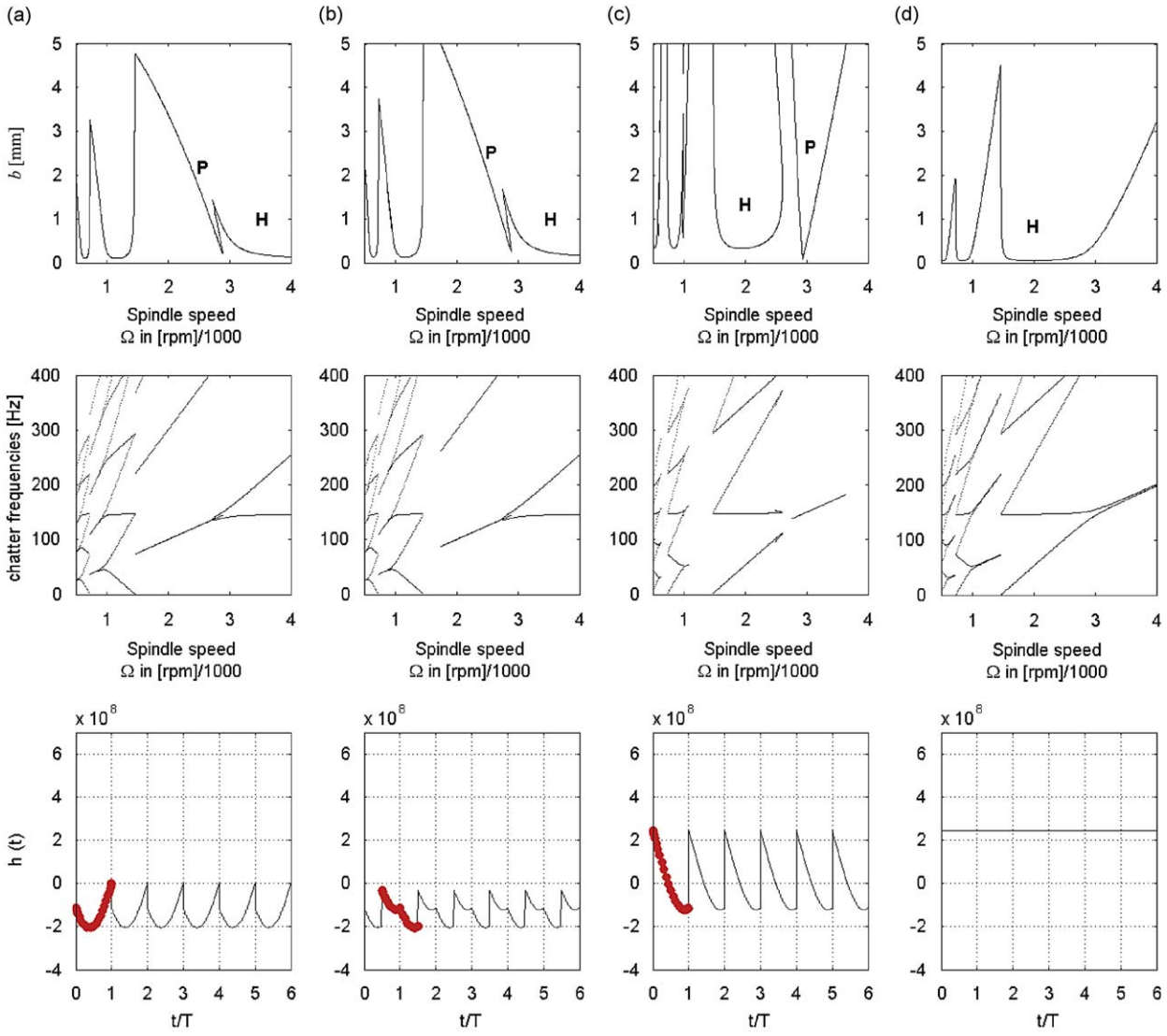

Fig. 12. Stability charts (first row), chatter frequencies (second row), and corresponding specific cutting force profiles (third row, where the thick line represents the segment that is approximated with Chebyshev collocation points) for 6 teeth, down-milling, and for $a/D = 0.25$ (column (a)), 0.50 (column (b)), 0.75 (column (c)), and 1 (column (d)).

and then it changes. As was shown in [40], the reason for that is the change of the sign of the average value of specific cutting force as the immersion ratio is varied. In the same reference, for both linear and nonlinear cutting force model, it was also shown that, with the increase of a/D, the major Hopf lobe at the right-hand side first shrinks, and then completely vanishes, defining the beginning of a local optimal stable interval, which corresponds to a range of radial immersion in which the stable portion of the parameter plane is the greatest. At some level of radial immersion, it appears to the left of the corresponding flip lobe (which indicates the end of the optimal stable interval defined in [40]). For 100 percent immersion ratio, the specific cutting force becomes constant, which means that this case can be handled like the problem of turning, in which the stability boundaries (which are only due to Hopf bifurcation) are the same for up- and down-milling and can be obtained analytically [46]. For the two examples of case (b) in Fig. 1 (i.e. the 75 percent immersion case in Fig. 11 and the 25 percent case in Fig. 12), the two-interval collocation expansion discussed in Section 4 was used.

Qualitatively similar results to those obtained in [40] are shown in Figs. 13 and 14 where the stability diagrams have been plotted for 16 immersion ratios between 0.61 and 0.76 for the case of 4 teeth (between 0.65 and 0.8 for the case of 6 teeth) using the parameters in Table 1. It can be seen that in both cases the major Hopf lobe at the far right-hand side shrinks such that it moves to the right and completely disappears by $a/D = 0.65$ for 4 teeth ($a/D = 0.68$ for 6 teeth). At the immersion ratio between 65 and 71 percent for 4 teeth (68 and 70 percent for 6 teeth) there is no major Hopf lobe to the right or left of the major flip lobe which is at 4400 rpm for 4 teeth (compare with Fig. 11) and at 2900 rpm for 6 teeth (compare with Fig. 12), while for 72 percent (71 percent) immersion the Hopf lobe suddenly appears to the left of the flip

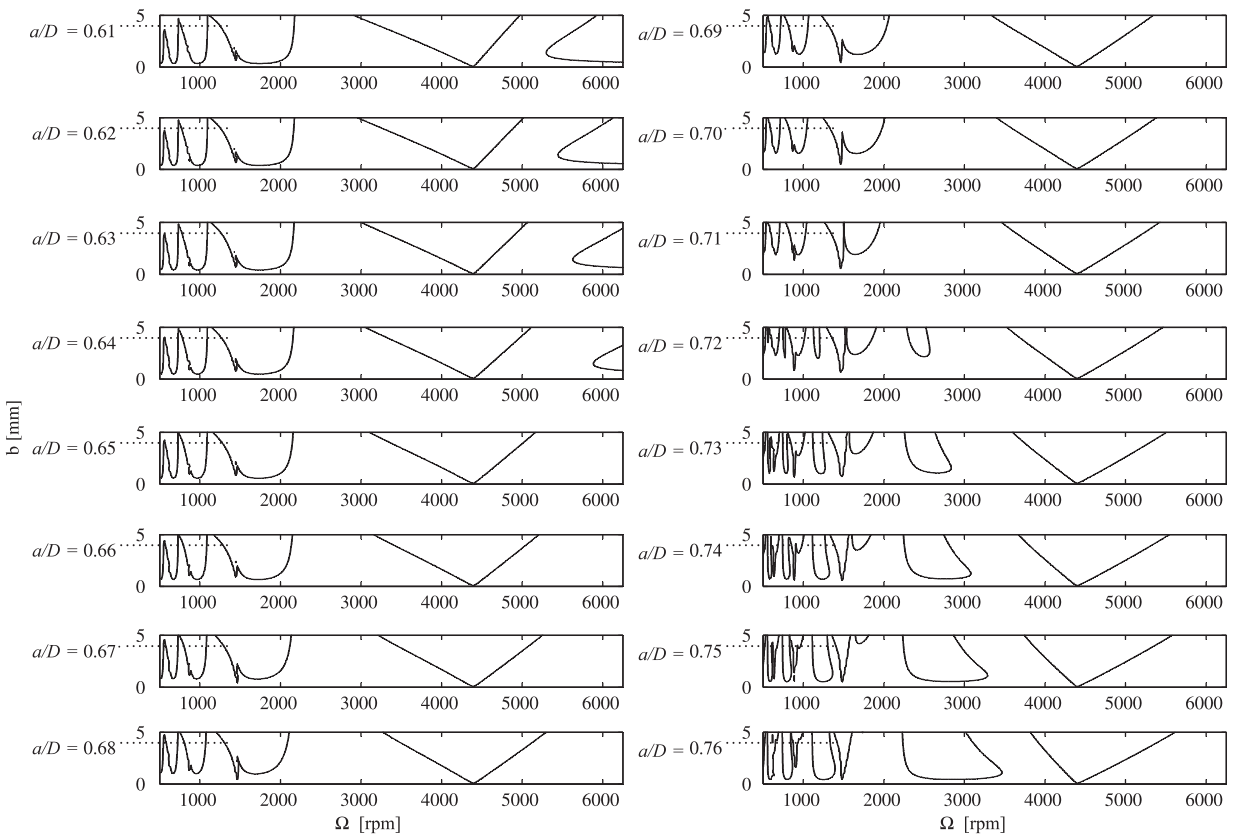

Fig. 13. Optimal stable immersion levels for down-milling with 4 cutting teeth and using the parameters in Table 1.

lobe. A further increase in the immersion level subsequently causes the lobe to drop even lower, dropping below $b = 2$ mm near 73 percent (72 percent) immersion. The main difference from prior results is that the optimal stable interval contracts as the number of simultaneously engaged teeth increases, which can be observed by comparing Figs. 13 and 14 with Fig. 7 in [40]. The change in stability characteristics above can be explained by computing the average value of $h(t)$ over a full period of rotation of the tool for z teeth (similar to the way this was done in [40] for a single tooth) from the following equation:

$$\langle h(t)\rangle = \frac{\Omega}{2\pi}\int_0^{2\pi/\Omega} h(t)\,\mathrm{d}t = \frac{zK_t}{2\pi}\int_{\theta^{\mathrm{enter}}}^{\theta^{\mathrm{exit}}} (\cos\theta + \tan\gamma\sin\theta)\sin\theta\,\mathrm{d}\theta. \tag{34}$$

Therefore, for z teeth, the average specific cutting force for up-milling is found as

$$\frac{\langle h(t)\rangle}{K_t} = \frac{z}{2\pi}\left\{\left(2\frac{a}{D}\left(1-\frac{a}{D}\right)\right) + \tan\gamma\left(\frac{1}{2}\cos^{-1}\left(1-2\frac{a}{D}\right) + \left(2\frac{a}{D}-1\right)\sqrt{\frac{a}{D}\left(1-\frac{a}{D}\right)}\right)\right\}, \tag{35}$$

while for down-milling it is

$$\frac{\langle h(t)\rangle}{K_t} = \frac{z}{2\pi}\left\{\left(-2\frac{a}{D}\left(1-\frac{a}{D}\right)\right) + \tan\gamma\left(\frac{\pi}{2} - \frac{1}{2}\cos^{-1}\left(2\frac{a}{D}-1\right) + \left(2\frac{a}{D}-1\right)\sqrt{\frac{a}{D}\left(1-\frac{a}{D}\right)}\right)\right\}. \tag{36}$$

These are plotted for 4, 6, and 8 teeth (up to 2, 3, and 4 teeth simultaneously engaged, respectively, see also Fig. 5) in Fig. 15. With no contrast to previous results, for $a/D>0$ and $\tan\gamma>0$, $\langle h(t)\rangle$ is always positive for up-milling, while for down-milling $\langle h(t)\rangle$ is negative for a/D less than a critical value and is positive for a/D greater than this value. It should be noted that while the presence of multiple teeth alters the average cutting force from that of a single tooth, the immersion ratio where it is zero for down-milling remains the same, which is seen in Fig. 15.

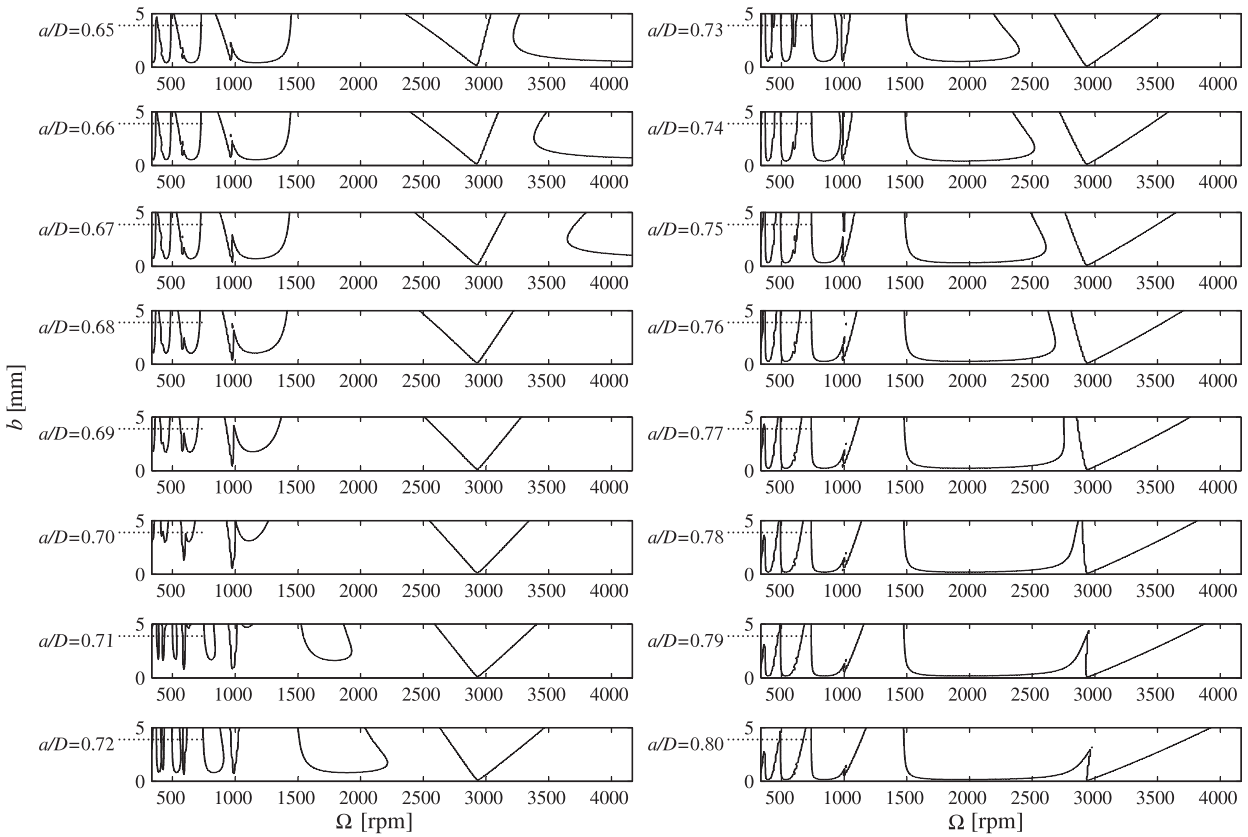

Fig. 14. Optimal stable immersion levels for down-milling with 6 cutting teeth and using the parameters in Table 1.

Table 1
Parameters used in the stability analysis.

Parameter	Value
m	2.5729 kg
ω_n	920.49 rad/s
ζ	0.0032
K_n	2.0×10^8 N/m^2
K_t	5.5×10^8 N/m^2
$\tan\gamma$	0.36

6. Analysis of chatter frequencies and stable periodic trajectories

The previous sections described the stability analysis of a milling process with multiple teeth simultaneously cutting. Consequently, the stable and unstable regions in the parameter space were graphed. Machining in the unstable range will cause the tool to chatter with certain frequencies. These chatter frequencies can be measured experimentally as well as determined analytically [50]. In Section 6.1, the expressions for finding the chatter frequencies are given and applied to cases with multiple teeth in the cut.

However, even in the absence of chatter, certain choices of the process parameters can result in stable periodic motions of the tool that will degrade the surface integrity of the workpiece. These stable periodic motions correspond to steady-state vibrations of the tool which are influenced by the cutting process parameters such as the spindle speed, the axial depth of cut, and the tool feed. A better parameter selection is hence achieved if both stability and the associated equilibrium solutions are considered during the process design. In Section 6.2, the stable periodic equilibrium solutions are determined via a Fourier series expansion and harmonic balance approach. The fixed points of the discrete map obtained through TFEA are then compared to the equilibrium solutions from the harmonic balance approach.

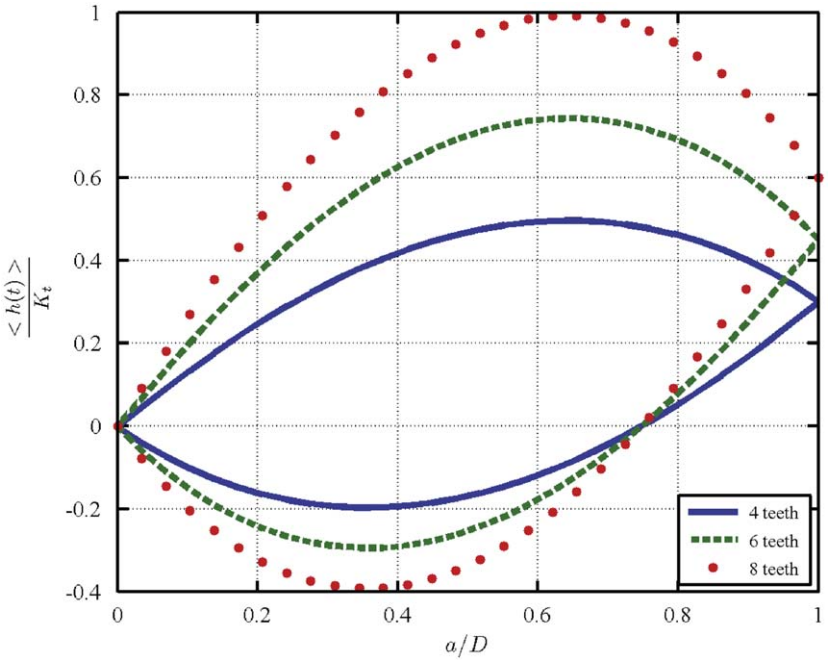

Fig. 15. Average cutting forces for up- (top curve) and down- (bottom curve) milling with $\tan\gamma = 0.3$ for 4 (solid), 6 (dashed), and 8 (dotted) teeth.

6.1. Chatter frequencies

The expressions for chatter frequencies occurring in milling processes were derived in Ref. [50] for the secondary Hopf and period-doubling bifurcation. For the secondary Hopf case, the chatter frequencies are given as

$$f_H = \left\{ \pm\omega + j\frac{2\pi}{\tau} \right\} [\text{rad/s}] = \left\{ \pm\frac{\omega}{2\pi} + j\frac{z\Omega}{60} \right\} [\text{Hz}], \quad j = \ldots, -1, 0, 1, \ldots, \tag{37}$$

where τ is given in seconds, and Ω in rpm with only the positive values of f_H having physical meaning. For the period-doubling case, the frequencies can be written in the simple form

$$f_{PD} = \left\{ \frac{\pi}{\tau} + j\frac{2\pi}{\tau} \right\} [\text{rad/s}] = \left\{ \pm\frac{z\Omega}{30} + j\frac{z\Omega}{60} \right\} [\text{Hz}], \quad j = \ldots, -1, 0, 1, \ldots \ . \tag{38}$$

Either the frequency set f_H or f_{PD} shows up during chatter. However, if Eq. (12) is stable, then these frequencies do not arise. Figs. 11 and 12 show chatter frequencies (second rows) corresponding to the stability charts and specific cutting force profiles above and below.

6.2. Periodic motion of the tool

This section investigates the periodic motion of the tool using two methods: (1) the harmonic balance, and (2) the fixed points of a discrete map. Previously, some aspects of these two methods were compared to ascertain the surface location error in milling [5,37,38]. However, these past investigations have only compared a single point in the time series which coincided with either the tool entry (for up-milling) or exit (for down-milling). A new feature of the current work is a quantitative comparison of the time series generated by both methods. As a consequence of the present study, the discrepancies between these methods are unveiled and explained.

6.2.1. Harmonic balance

The equation of motion for a single degree-of-freedom milling operation was introduced in Eq. (6). This equation can be re-written as

$$\ddot{x}(t) + 2\zeta\omega_n\dot{x}(t) + \omega_n^2 x(t) = \omega_n^2\left[-\frac{bh(t)}{k}[x(t) - x(t-\tau)] - \frac{bf_0(t)}{k} \right].$$

However, for a chatter-free machining process, the tool oscillations are assumed to be τ- periodic, i.e. $x(t) = x(t-\tau)$ [5,24,43,61]; therefore, the above equation reduces to

$$\ddot{x}(t) + 2\zeta\omega_n\dot{x}(t) + \omega_n^2 x(t) = \omega_n^2\tilde{f}_0(t), \tag{39}$$

where $\tilde{f}_0(t) = -bf_0(t)/k$. The solutions of Eq. (39) represent the stable periodic motions of the system, and

$$\tilde{f}_0(t) = -\frac{1}{k}\sum_{p=1}^{z} bK_t g_p(t)[\cos\theta_p(t) + \tan\gamma\sin\theta_p(t)]f\sin\theta_p(t) \tag{40}$$

is only piece-wise continuous. A continuous representation of $\tilde{f}_0(t)$ is obtained by assuming that $\tilde{f}_0(t)$ is T-periodic for a stable motion and expressing it by a complex Fourier series according to [43]

$$\tilde{f}_0(t) = \sum_{r=1}^{z}\sum_{n=-\infty}^{\infty} \Gamma_n \mathrm{e}^{\mathrm{i}(n\Omega t-\theta_r)}, \tag{41}$$

where $\theta_r = (r-1)2\pi/z$. For instance, for a four-tooth cutter with evenly spaced teeth we obtain $\theta_1 = 0$, $\theta_2 = \pi/2$, $\theta_3 = \pi$, and $\theta_4 = 3\pi/2$.

Furthermore, owing to the linearity of Fourier series, Eq. (41) was obtained by combining the individual Fourier series representations of each tooth then factoring out the identical Fourier coefficients. Indeed, these Fourier coefficients can be calculated from

$$\Gamma_0 = \frac{1}{T}\int_{t_{\mathrm{en}}}^{t_{\mathrm{ex}}} \tilde{f}_0(t)\,\mathrm{d}t, \tag{42a}$$

$$\Gamma_n = \frac{1}{T}\int_{t_{\mathrm{en}}}^{t_{\mathrm{ex}}} \tilde{f}_0(t)\mathrm{e}^{-\mathrm{i}n\Omega t}\,\mathrm{d}t, \quad n = \pm(1,2\ldots,\infty), \tag{42b}$$

where $t_{\mathrm{en}} = \theta^{\mathrm{enter}}/\Omega$ and $t_{\mathrm{ex}} = \theta^{\mathrm{exit}}/\Omega$, and Ω is the angular velocity expressed in (rad/s). Since the excitation in Eq. (39) was assumed to be periodic, the steady-state response, $\overline{x}(t)$, will also be periodic and it can be represented by another Fourier series of the form

$$\overline{x}(t) = \sum_{r=1}^{z}\sum_{n=-\infty}^{\infty} X_n \mathrm{e}^{\mathrm{i}(n\Omega t-\theta_r)}. \tag{43}$$

Making use of the frequency response function notation, and substituting Eqs. (41) and (43) into Eq. (39) yields

$$\overline{x}(t) = \sum_{r=1}^{z}\sum_{n=-\infty}^{\infty} G(n\Omega)\Gamma_n \mathrm{e}^{\mathrm{i}(n\Omega t-\theta_r)}, \tag{44}$$

where the frequency response function is given by

$$G(n\Omega) = \frac{\omega_{\mathrm{n}}^2}{\omega_{\mathrm{n}}^2 - (n\Omega)^2 + \mathrm{i}2\zeta\omega_{\mathrm{n}}(n\Omega)}. \tag{45}$$

In fact, Eq. (44) can be written as

$$x(t) = N\Gamma_0 + \sum_{r=1}^{z}\sum_{n=1}^{\infty}(G(n\Omega)\Gamma_n \mathrm{e}^{\mathrm{i}(n\Omega t-\theta_r)} + \hat{G}(n\Omega)\hat{\Gamma}_n \mathrm{e}^{-\mathrm{i}(n\Omega t-\theta_r)}), \tag{46}$$

where $\hat{G}(n\Omega)$ and $\hat{\Gamma}_n$ denote the complex conjugates of $G(n\Omega)$ and Γ_n, respectively.

6.2.2. Map fixed points

The governing equation of motion for a milling operation was introduced in Eq. (6). This equation can be represented in state-space form as

$$\dot{\mathbf{x}} = \mathbf{R}(t)\mathbf{x}(t) + \mathbf{L}(t)\mathbf{x}(t-\tau) + \mathbf{c}(t), \tag{47a}$$

where $\mathbf{R}(t)$ and $\mathbf{L}(t)$ are the same as in Eq. (12), and

$$\mathbf{c}(t) = \begin{bmatrix} 0 \\ -\dfrac{bf_0(t)}{m} \end{bmatrix}. \tag{47b}$$

TFEA approach is applied to Eq. (47) by approximating the solution $\mathbf{x}$ as a linear combination of polynomials—similar to Eq. (16). The approximate solution is then substituted into Eq. (47) and the method of weighted residuals is used to reduce the approximation error. Following the steps of Section 3, a discrete dynamic map over one period is created according to [5,24]

$$\mathbf{H}\mathbf{m}_{\mathbf{x}}(n) = \mathbf{G}\mathbf{m}_{\mathbf{x}}(n-1) + \mathbf{q}, \tag{48}$$

where $\mathbf{m}_{\mathbf{x}}(n)$ is similar to $\mathbf{m}_n$ in Eq. (24), except that it represents the temporal finite element expansion of the state vector $\mathbf{x}$ itself rather than of its perturbation ξ. $\mathbf{H}$ and $\mathbf{G}$ were defined in Eq. (24), and, using two temporal elements, the entries of

the vector $\mathbf{q} = [\mathbf{0}\ \mathbf{d}_1^1\ \mathbf{d}_2^1\ \mathbf{d}_1^2\ \mathbf{d}_2^2]^T$ are given by

$$\mathbf{d}_p^j = \int_0^{t_j} \mathbf{c}(\sigma + (j-1)t_j)\psi_p(\sigma)\,\mathrm{d}\sigma, \tag{49}$$

where $\mathbf{c}$ is given in Eq. (47). The fixed points of the map are associated with the stable periodic motion of the system and they are denoted by $\mathbf{m}_{\mathbf{x}}^*$. They occur when $\mathbf{m}_{\mathbf{x}}(n) = \mathbf{m}_{\mathbf{x}}(n-1)$ and they can be obtained from

$$\mathbf{m}_{\mathbf{x}}^*(n) = (\mathbf{G} - \mathbf{H})^{-1}\mathbf{q}, \tag{50}$$

or equivalently $\mathbf{m}_{\mathbf{x}}^*(n) = (\mathbf{I} - \mathbf{U})^{-1}(\mathbf{G}^{-1}\mathbf{q})$, where $\mathbf{U}$ is the monodromy operator defined in Eq. (15).

Whereas the harmonic balance approach represents a continuous approximation of the discontinuous cutting forces, the map's fixed points are obtained through discretizing the equation of motion. The fixed points obtained by Eq. (50) are compared to the results of the harmonic balance approach in Fig. 16 for up-milling and Fig. 17 for down-milling. The two figures are for an 8-tooth cutter with 50 percent radial immersion. In Fig. 16a, the time series of the tool oscillations over one period is plotted for both the harmonic balance approach and the fixed points of the dynamic map. It can be seen that the time series obtained with the two different approaches are in agreement. Graphs (b)–(d) compare the phase space obtained through harmonic balance (solid line) with an increasing number of harmonics to the results from the map's fixed points. Graph (b) shows that for a lower number of harmonics the harmonic balance approach has not converged close to a

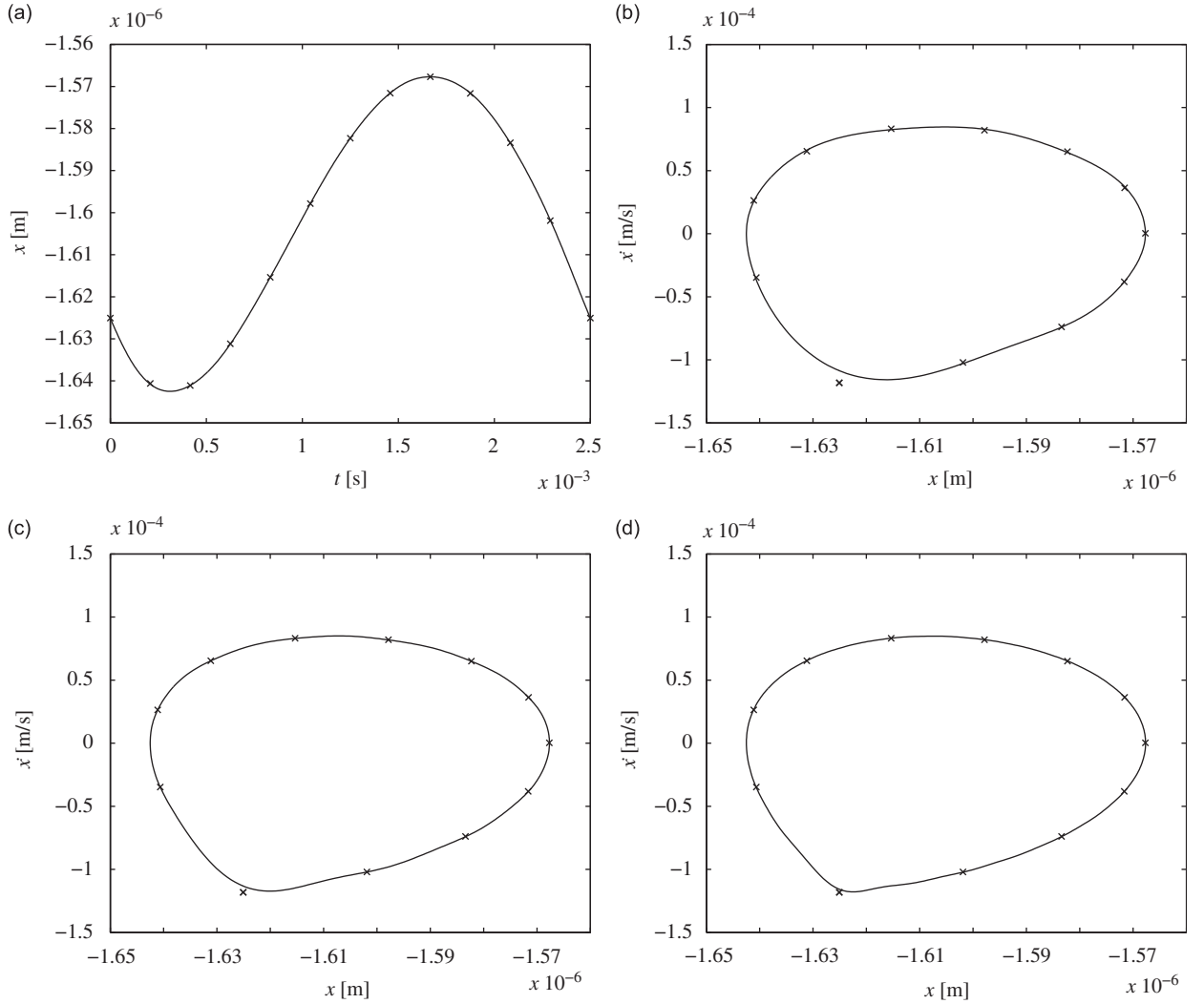

Fig. 16. The periodic solutions of an up-milling process with an 8-tooth cutter, 0.5 radial immersion, $\Omega = 3000$ rpm and $b = 0.5$ mm. In graph (a), 50 harmonics are used to plot the harmonic balance solution (solid line) against the fixed points (crosses) of the dynamic map over one period of oscillations. The phase space obtained by the fixed points of the map is also overlaid by the harmonic balance approach results (solid line) using (b) 50 harmonics, (c) 100 harmonics, and (d) 250 harmonics. In all the plots, 12 temporal elements were used to discretize the equation of motion.

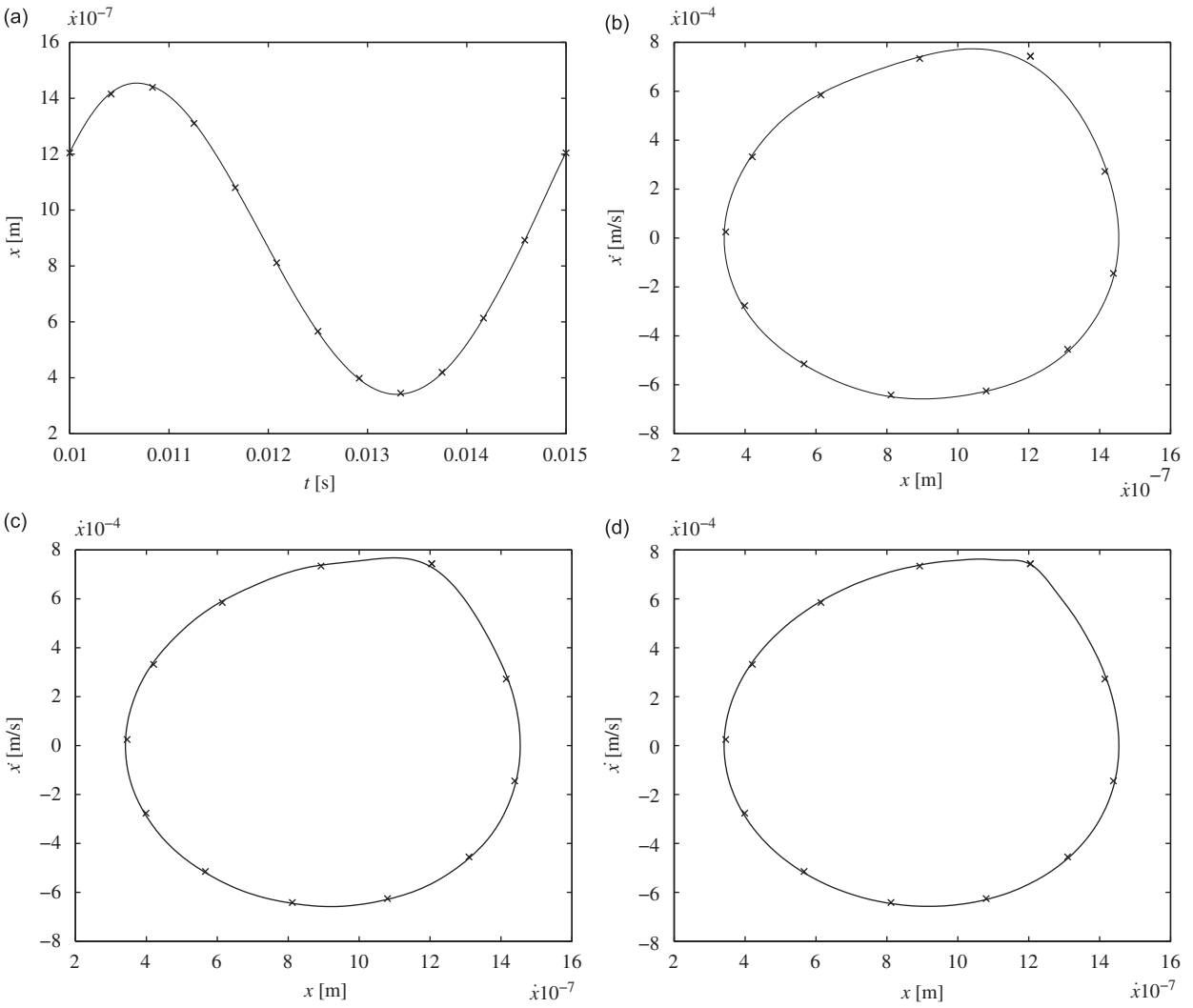

Fig. 17. The periodic solutions of a down-milling process with an 8-tooth cutter, 0.5 radial immersion, $\Omega = 1500$ rpm and $b = 1$ mm. In graph (a), 50 harmonics are used to plot the harmonic balance solution (solid line) against the fixed points (crosses) of the dynamic map over one period of oscillations. The phase space obtained by the fixed points of the map is also overlaid by the harmonic balance approach results (solid line) using (b) 50 harmonics, (c) 100 harmonics, and (d) 250 harmonics. In all the plots, 12 temporal elements were used to discretize the equation of motion.

certain point. This point coincides with the cutting force discontinuity at the beginning of the cut. However, as the number of harmonics is increased in graphs (c)–(d), the harmonic balance results approach their discretization approach counterparts. Fig. 16 shows that whereas the TFEA approach yielded convergent results, the harmonic balance approach required a larger number of harmonics to converge to the correct response behavior. This is shown in a series of plots where the number of harmonics has been increased until the results of the harmonic balance method approached those of TFEA. Similar conclusions can be drawn from Fig. 17 for a down-milling operation.

7. Conclusions

This paper investigated the milling process with multiple teeth simultaneously cutting. Two semi-analytical techniques, namely the Chebyshev collocation method and TFEA, were extended to obtain the stability diagrams of multi-tooth cutters using different radial immersions; chatter frequency diagrams were also obtained to give the complete stability picture. Both methods yielded identical stability charts and were able to replicate the results from prior works.

In contrast to one or two teeth in the cut, multiple teeth engagement with three or more teeth was found to give rise to smaller regions of period-doubling instability at all partial radial immersion levels. While the superposition of the cutting forces results in a constant specific cutting force, for the full immersion case, an additional effect is the disappearance of the

period-doubling lobes. An increase in the number of engaged teeth further decreases the strength of higher harmonics in the force profile that lead to a period doubling bifurcation—even for lower values of radial immersion.

In addition, the case of simultaneously engaged teeth was found to demonstrate rapid transitions in the stability lobes for relatively small changes in the radial immersion ratio. For example, the stability diagram in Fig. 13, for a 4-tooth cutter, shows that the largest Hopf lobe undergoes sharp transitions for relatively small variations in the radial immersion. As a second example, Fig. 14 shows the same observation for a 6-tooth cutter. These rapid transitions in the stability lobes for multiple teeth simultaneously cutting have been linked to the sign change in the average specific cutting force.

Finally, the stable periodic motion of the tool was investigated using two different methods. The first method is a harmonic balance approach that uses a continuous approximation of the discontinuous cutting forces via a Fourier series expansion; the second method uses the fixed points of the dynamic map created by the TFEA approach. Although both time series matched, a large number of harmonics were required for the harmonic balance approach to converge to the correct values. Therefore, for calculating the periodic solutions of discontinuous delay systems, a discretization approach was shown to be more efficient than a Fourier expansion.

Acknowledgments

Support from US National Science Foundation with Grants nos. CMMI-0900289 and CMMI-0900266 is gratefully acknowledged.

References

[1] J. Tlusty, A. Polacek, C. Danek, J. Spacek, *Selbsterregte Schwingungen an Werkzeugmaschinen*, VEB Verlag Technik, Berlin, 1962.
[2] S.A. Tobias, *Machine Tool Vibration*, Blackie, London, 1965.
[3] J. Tlusty, *Manufacturing Processes and Equipment*, 1st ed., Prentice-Hall, Upper Saddle River, NJ, 2000.
[4] Y. Altintaş, *Manufacturing Automation*, 1st ed., Cambridge University Press, New York, NY, 2000.
[5] B.P. Mann, P.V. Bayly, M.A. Davies, J.E. Halley, Limit cycles, bifurcations, and accuracy of the milling process, *Journal of Sound and Vibration* 277 (2004) 31–48.
[6] S. Doi, S. Kato, Chatter vibration of lathe tools, *Transactions of the ASME* 78 (1956) 1127–1134.
[7] F. Taylor, On the art of cutting metals, *Transactions of ASME* 43 (1907) 31–350.
[8] J. Tlusty, M. Polacek, The stability of machine tools against self-excited vibrations in machining, Proceedings of the ASME International Research in Production Engineering, 1963, pp. 465–474.
[9] H.E. Merrit, Theory of self-excited machine-tool chatter, *Journal of Engineering for Industry* 87 (4) (1965) 447–454.
[10] G. Stépán, *Retarded Dynamical Systems: Stability and Characteristic Functions*, Wiley, New York, 1989.
[11] T. Insperger, G. Stépán, P.V. Bayly, B.P. Mann, Multiple chatter frequencies in milling processes, *Journal of Sound and Vibration* 262 (2) (2003) 333–345.
[12] J. Gradišek, E. Govekar, I. Grabec, Time series analysis in metal cutting: chatter versus chatter-free cutting, *Mechanical Systems and Signal Processing* 12 (6) (1998) 839–854.
[13] J. Gradišek, E. Govekar, I. Grabec, Using coarse-grained entropy rate to detect chatter in cutting, *Journal of Sound and Vibration* 214 (5) (1998) 941–952.
[14] T. Schmitz, M. Davies, K. Medicus, J. Snyder, Improving high-speed machining material removal rates by rapid dynamic analysis, *CIRP Annals—Manufacturing Technology* 50 (1) (2001) 263–268.
[15] G. Yucesan, Y. Altintaş, Improved modeling of cutting force coefficients in peripheral milling, *International Journal of Machine Tools and Manufacture* 34 (4) (1994) 473–487.
[16] T. Insperger, G. Stépán, Updated semi-discretization method for periodic delay-differential equations with discrete delay, *International Journal for Numerical Methods* 61 (2004) 117–141.
[17] X.H. Long, B. Balachandran, B. Mann, Dynamics of milling processes with variable time delay, Nonlinear Dynamics 47 (1) (2007) 49–63.
[18] H. Ma, E.A. Butcher, E. Bueler, Chebyshev expansion of linear and piece-wise linear dynamic systems with time delay and periodic coefficients under control excitations, *Journal of Dynamic Systems, Measurement, and Control* 125 (2003) 236–243.
[19] E.A. Butcher, H. Ma, E. Bueler, V. Averina, Z. Szabó, Stability of linear time-periodic delay-differential equations via Chebyshev polynomials, *International Journal Numerical Methods in Engineering* 59 (2004) 895–922.
[20] V. Deshmukh, H. Ma, E.A. Butcher, Optimal control of parametrically excited linear delay differential systems via Chebyshev polynomials, *Optimal Control Applications and Methods* 27 (2006) 123–136.
[21] K. Engelborghs, T. Luzyanina, K.J. in 'T Hout, D. Roose, Collocation methods for the computation of periodic solutions of delay differential equations, *SIAM Journal on Scientific Computing* 22 (2000) 1593–1609.
[22] J.H. Argyris, D.W. Scharpf, Finite elements in time and space, *Aeronautical Journal of the Royal Society* 73 (1969) 1041–1044.
[23] M. Borri, C. Bottasso, P. Mantegazza, Basic features of the time finite element approach for dynamics, *Meccanica* 27 (1992) 119–130.
[24] B.P. Mann, N.K. Garg, K.A. Young, A.M. Helvey, Milling bifurcations from structural asymmetry and nonlinear regeneration, *Nonlinear Dynamics* 42 (4) (2005) 319–337.
[25] B.R. Patel, B.P. Mann, K.A. Young, Uncharted islands of chatter instability in milling, *International Journal of Machine Tools and Manufacture* 48 (2008) 124–134.
[26] R. Faassen, N. Van de Wouw, J. Oosterling, H. Nijmeijer, Prediction of regenerative chatter by modelling and analysis of high-speed milling, *International Journal of Machine Tools and Manufacture* 43 (2003) 1437–1446.
[27] E. Budak, Y. Altintaş, Analytical prediction of chatter stability conditions for multi-degree of systems in milling. Part I: modelling, *Journal of Dynamic Systems, Measurement and Control* 120 (1998) 22–30.
[28] S.D. Merdol, Y. Altintaş, Multi frequency solution of chatter stability for low immersion milling, *Journal of Manufacturing Science and Engineering* 126 (3) (2004) 459–466.
[29] S. Smith, J. Tlusty, An overview of the modeling and simulation of the milling process, *Journal of Engineering for Industry* 113 (1991) 169–175.
[30] D. Montgomery, Y. Altintaş, Mechanism of cutting force and surface generation in dynamic milling, *Journal of Engineering for Industry* 113 (1991) 160–168.
[31] M.X. Zhao, B. Balachandran, Dynamics and stability of milling process, *International Journal of Solids and Structures* 38 (10–13) (2001) 2233–2248.
[32] Y. Altintaş, E. Budak, Analytical prediction of stability lobes in milling, *CIRP Annals* 44 (1) (1995) 357–362.
[33] M.A. Davies, J.R. Pratt, B. Dutterer, T.J. Burns, Stability prediction for low radial immersion milling, *Journal of Manufacturing Science and Engineering* 124 (2) (2002) 217–225.

[34] I. Minis, R. Yanushevsky, A new theoretical approach for prediction of machine tool chatter in milling, *Journal of Engineering for Industry* 115 (1993) 1–8.
[35] T. Insperger, G. Stépán, Stability of the milling process, *Periodica Polytechnica* 44 (1) (2000) 47–57.
[36] T. Insperger, B.P. Mann, G. Stépán, P.V. Bayly, Stability of up-milling and down-milling, Part 1: alternative analytical methods, *International Journal of Machine Tools and Manufacture* 43 (2003) 25–34.
[37] B.P. Mann, K.A. Young, T.L. Schmitz, D.N. Dilley, Simultaneous stability and surface location error predictions in milling, *Journal of Manufacturing Science and Engineering* 127 (2005) 446–453.
[38] T. Schmitz, B. Mann, Closed form solutions for the prediction of surface location error in milling, *International Journal of Machine Tools and Manufacture* 46 (2006) 1369–1377.
[39] E.A. Butcher, P. Nindujarla, E. Bueler, Stability of up- and down-milling using Chebyshev collocation method, Proceedings of 5th International Conference on Multibody Systems, Nonlinear Dynamics, and Control, ASME DETC'05, Long Beach, CA, September 24–28, 2005.
[40] E.A. Butcher, O.A. Bobrenkov, E. Bueler, P. Nindujarla, Analysis of milling stability by the Chebyshev collocation method: algorithm and optimal stable immersion levels, *Journal of Computational and Nonlinear Dynamics* 4 (2009) 1–12 031003.
[41] M.A. Davies, J.R. Pratt, B. Dutterer, T.J. Burns, The stability of low immersion milling, *Annals of the CIRP* 49 (2000) 37–40.
[42] P.V. Bayly, J.E. Halley, B.P. Mann, M.A. Davis, Stability of interrupted cutting by temporal finite element analysis, *Journal of Manufacturing Science and Engineering* 125 (2003) 220–225.
[43] B.P. Mann, B.T. Edes, S.J. Easley, K.A. Young, K. Ma, Chatter vibration and surface location error prediction for helical end mills, *International Journal of Machine Tools and Manufacture* 48 (2008) 350–361.
[44] B.P. Mann, T. Insperger, P.V. Bayly, G. Stépán, Stability of up-milling and down-milling, Part 2: experimental verification, *International Journal of Machine Tools and Manufacture* 43 (2003) 35–40.
[45] B. Balachandran, Non-linear dynamics of milling process, *Proceedings of the Royal Society of London A* 359 (2001) 793–819.
[46] R. Szalai, G. Stépán, Lobes and lenses in the stability chart of interrupted turning, *Journal of Computational and Nonlinear Dynamics* 1 (2006) 205–211.
[47] P.V. Bayly, J.E. Halley, B.P. Mann, M.A. Davis, Stability of interrupted cutting by temporal finite element analysis, *Journal of Manufacturing Science and Engineering* 125 (2003) 220–225.
[48] H. Opitz, F. Bernardi, Investigation and calculation of the chatter behavior of lathes and milling machines, *Annals of the CIRP* 18 (1970) 335–343.
[49] Y.N. Sankin, The stability of milling machines during cutting, *Soviet Engineering Research* 4 (1984) 40–43.
[50] T. Insperger, G. Stépán, P.V. Bayly, B.P. Mann, Multiple chatter frequencies in milling processes, *Journal of Sound and Vibration* 262 (2003) 333–345.
[51] B. Mann, K. Young, An empirical approach to stability and parametric identification in time delayed dynamical systems, *Proceedings of the Royal Society of London A* 462 (2006) 2145–2160.
[52] B. Mann, B. Patel, Stability of delay equations written as state space models, Journal of Vibration and Control (2008), accepted for publication.
[53] L.N. Trefethen, *Spectral Methods in Matlab*, SIAM Press, Philadelphia, 2000.
[54] B.P. Mann, K.A. Young, An empirical approach for delayed oscillator stability and parametric identification, *Proceedings of the Royal Society A* 462 (2006) 2145–2160.
[55] L. Fox, I.B. Parker, *Chebyshev Polynomials in Numerical Analysis*, Oxford University Press, London, 1968.
[56] E. Bueler, Error bounds for approximate eigenvalues of periodic-coefficient linear delay differential equations, *SIAM Journal of Numerical Analysis* 45 (6) (2007) 2510–2536.
[57] E. Bueler, Guide to DDEC: stability of linear, periodic DDEs using the DDEC suite of Matlab codes, 2005.
[58] V. Deshmukh, E.A. Butcher, E. Bueler, Dimensional reduction of nonlinear delay differential equations with periodic coefficients using Chebyshev spectral collocation, *Nonlinear Dynamics* 52 (2007) 137–149.
[59] V. Deshmukh, Spectral collocation-based optimization in parameter estimation for nonlinear time-varying dynamical systems, *Journal of Computational and Nonlinear Dynamics* 3 (1–7) (2008) 011010.
[60] N. Sims, B. Mann, S. Huyanan, Analytical prediction of chatter stability for variable pitch and variable helix milling tools, *Journal of Sound and Vibration* 317 (2008) 664–686.
[61] T. Insperger, J. Gradišek, M. Kalveram, G. Stépán, K. Winert, E. Govekar, Machine tool chatter and surface location error in milling processes, *Journal of Manufacturing Science and Engineering* 128 (2006) 913–920.